NUMERICAL SIMULATION AND PERFORMANCE OPTIMIZATION OF PEROVSKITE SOLAR CELL

A THESIS IN

ELECTRICAL ENGINEERING

Presented to the Faculty of the University
Of Missouri-Kansas City in partial fulfillment of
The requirements for the degree

MASTER OF SCIENCE

BY

SAI NAGA RAGHURAM NANDURI

B.TECH., Koneru Lakshmaiah University, Vijayawada, 2015

Kansas City, Missouri

2017

NUMERICAL SIMULATION AND PERFORMANCE OPTIMIZATION OF PEROVSKITE SOLAR CELL

Sai Naga Raghuram Nanduri, Candidate for the Master of Science Degree

University Of Missouri-Kansas City, 2017

ABSTRACT

The organic-metal halide perovskite is emerging technology in photo voltaic solar cells. For any solar cell to get the significant efficiency depends on various design parameters such as material thickness, device architecture, doping concentration etc.. There are many solar cell simulation software which can be used to carry out simulation and thus optimization based on those parameters. Here for this research, we have used wxAMPS because it is freely available, simple, efficient and quite popular in solar cell research society. The software has been used to simulate for single junction as well as multijunction/tandem solar cell. Keeping external parameters constant (one-sun, AM1.5G solar radiation, 1000 w/m^2 irradiation), numerical simulation and analysis of a perovskite solar cell with a single junction configuration of ETM/Perovskite/HTM and a tandem (double junction) configuration of ETM/Perovskite/HTM/Recombination layer/ ETM/Perovskite/HTM were carried out. In the proposed single junction configuration Zinc oxide (ZnO) was used as Electron Transport Material (ETM) as), mixed halide perovskite (CH3NH3PbI3-xClx) was used as absorber material, and Copper thiocyanate (CuSCN) was used as Hole transport material (HTM). Then simulation of double junction tandem solar cell was performed. Tandem cells are solar cells

made of multiple junctions with tunable absorbing materials, which aim to overcome the Shockley-Queisser limit of single junction solar cells. Recently, organic-inorganic hybrid perovskite solar cells have stirred enormous interest as ideal candidates for tandem solar cells, due to high open circuit voltage, relatively wide optical bandgap, and low temperature solution processibility. In this research a new architecture of perovskite/perovskite tandem solar cell was explored. In this architecture two different types of single junction perovskite solar cells were used for the tandem structure. ZnO/$CH_3NH_3PbI_{3-x}Cl_x$/CuSCN solar cell was employed as a top cell and ZnO/$MAPbBr_3$/$MAPbI_3$/CuSCN was employed as bottom cell. The simulation results shows a significant enhancement in conversion efficiency when compared to individual single junction perovskite solar cells. These simulation results can help researchers to reasonably choose materials and optimally design high performance perovskite single and tandem/multijunction solar cells.

APPROVAL PAGE

The faculty listed below, appointed by the Dean of the School of Computing and Engineering have examined a thesis titled " Numerical Simulation and Performance Optimization of Perovskite Solar Cell" presented by Nanduri Sai Naga Raghuram Nanduri, candidate for the Master of Science degree, and certify that in their opinion it is worthy of acceptance.

Supervisory Committee

Dr. Ghulam M. Chaudhry, Committee Chair

Department Chair of Computer Science Electrical Engineering

Dr. Mahbube K. Siddiki

Department of Computer Science Electrical Engineering

Prof. Kevin P. Kirkpatrick

Department of Computer Science Electrical Engineering

ACKNOWLEDGEMENTS

I would like to take this opportunity to express my profound thanks to those who helped me with a various aspect of conducting research and pursuing my degree.

First and foremost, I would like to thank my Research advisor Dr. Mahbube K. Siddiki who helped me a lot in my academic and research activity from the beginning of my graduate study. Without his cooperation and helpful suggestions, it was not possible to complete my research and study. The door to Dr. Siddiki office was always open whenever I ran into a trouble or had a question about my research. I am grateful to him for his wise advice that gave the opportunity to learn things professionally.

Next, I would also like to thank Dr. Ghulam M. Chaudhry for continually providing me with guidance and opportunity. His friendly and supportive method to motive the students is very helpful to conduct the research in a very efficient way. I would like to thank my defense committee member professor. Kevin P. Kirkpatrick for his time and kind feedback.

My special thanks to my wonderful parents, my brothers, sisters and friends who helped me throughout the process of completing my degree. Their patience, kindness, and encouragement made me optimistic to pursue my dream towards higher study.

Finally, I would like to extend my appreciation to all stuffs of CSEE department of UMKC for their help.

CONTENTS

LIST OF TABLES

Table Page

LIST OF ILLUSTRATIONS

Figure Page

CHAPTER 1

INTRODUCTION

1.1 Background

The humankind needs energy to exist. This energy is constantly produced through technologies that have evolved over time. One of the main factors that characterize the production of energy is the resource that is being exploited. The resources available can be divided in two main categories: non-renewable and renewable. In the first category are included all the sources of energy that can be exploited in a finite quantity, or with are generation time long enough to be considered finite in quantity. Coal, natural gases, petroleum and its derivatives, radioactive elements[1]. All these resources are in the first category. The amount of energy that can be obtained from these resources is in generally high. In second category, all the resources with an instantaneous regeneration are included, which means inexhaustible sources of energy. Tides, geothermal, hydroelectricity, wind and solar are the main sources of renewable energy[2]. The energy currently obtained from these resources is generally lower compared to non-renewable, however the idea of a theoretically inexhaustible source of energy attracts a lot of attention, especially in sight of a possible depletion of non-renewable sources [3]. Researchers, scientists and industries have collaborated over the years to find an answer to the constant demand of energy. Nowadays, the modern sources of energy implemented in everyday life are the results of years of study, research development and, finally, industrialized processes. Among all the different sources, both renewable or not, solar energy has always attracted a lot of interests. The energy provided by the Sun in the form of light is something natural as clearly shown in photosynthesis. The idea to convert sunlight into a usable form of energy is the base concept of the solar cell. The solar cell is an optoelectronic

device able to convert light into electric current, both the direct Sun light and also artificial or ambient light. However, the term light is referred here as the electromagnetic radiation emitted by the Sun on to the surface of the Earth. The Sun emits electromagnetic waves all over the spectrum of frequencies like a black body with a calculated temperature of 5777 K [4].

1.2 Evolution and History of Solar Cells

1839: Photovoltaic Effect Is Discovered. French scientist Edmond Becquerel first discovered the photovoltaic effect in 1839. This process occurs when light is absorbed by a material and creates electrical voltage. Most modern solar cells use silicon crystals to attain this effect.

1873–1876: Selenium's Photoconductivity Is Discovered. English electrical engineer Willoughby Smith discovered the photoconductivity of selenium, meaning it becomes electrically conductive when it absorbs light. Three years later, William Grylls Adams and Richard Evans Day learned that selenium could produce electricity from light without heat or moving parts that could easily break down. This discovery proved that solar power was easy to harvest and maintain, requiring fewer parts than other energy sources such as coal-fired plants.

1883: First Solar Cell Is Created New York inventor Charles Fritts created the first solar cell by coating selenium with a thin layer of gold. This cell achieved an energy conversion rate of 1–2%. Most modern solar cells work at an efficiency of 15–20%.

1887: The Photoelectric Effect Is Observed German physicist Heinrich Hertz first observed the photoelectric effect, where light is used to free electrons from a solid surface (usually metal) to create power. Contrary to expected results, Hertz found this process produced more power when exposed to ultraviolet light, rather than more intense visible light.

Albert Einstein later received the Nobel Prize for further explaining the effect. Modern-day solar cells rely on the photoelectric effect to convert sunlight into power.

1953–1956: Silicon Solar Cells Are Produced Commercially. Physicists at Bell Laboratories discovered that silicon is more efficient than selenium, creating the first practical solar cell now 6% efficient. This discovery led to solar cells capable of powering electrical equipment. In 1956, Western Electric began selling commercial licenses for its silicon PV technologies, but the prohibitive costs of silicon solar cells keep them from widespread market saturation.

1958: Solar Energy Is Used In Space. After years of experiments to improve the efficiency and commercialization of solar power, solar energy gained support when the government used it to power space exploration equipment. The first solar-powered satellite, Vanguard 1, has traveled more than 197,000 revolutions around Earth in the 50 years it has been in orbit. This application paved the way for more research to decrease costs and increase production.

1970s: Research Drives Costs Down. As oil prices rose in the 1970s, demand for solar power increased. Exxon Corporation financed research to create solar cells made from lower-grade silicon and cheaper materials, pushing costs from $100 per watt to only $20–$40 per watt. The federal government also passed several solar-friendly bills and initiatives and created the National Renewable Energy Laboratory (NREL) in 1977.

1982: The First Solar Parks Are Created. Arco Solar built the first solar park basically a solar power plant in Hesperia, California, in 1982. This park generated 1 megawatt, or 1,000 kilowatts per hour, while operating at full capacity. This could power a 100-kilowatt lightbulb for 10 hours. In 1983, Arco Solar built a second solar park in Carrizo Plains, California. At the

time, it was the largest collection of solar arrays in the world, containing 100,000 PV arrays that generated 5.2 megawatts at full capacity. While these plants fell into disarray with oil's return to popularity, they demonstrated the potential for commercial solar power production.

1995: Retractable RV Solar Panels Created. Solar research continued to expand into other commercial industries: Thomas Faludy filed a patent in 1995 for a retractable awning with integrated solar cells. This was one of the first times solar cells were used in recreational vehicles. Today, this feature is a popular way to power RVs**.**

1994–1999: Photovoltaic Conversion Reaches New Levels. In 1994, the National Renewable Energy Laboratory developed a new solar cell from gallium indium phosphide and gallium arsenide that exceeded 30% conversion efficiency. By the end of the century, the laboratory created thin-film solar cells that converted 32% of the sunlight it collected into usable energy.

2005: DIY Solar Panels Become Popular. As technology and efficiency of solar cells have increased, residential solar power has become more popular. DIY solar panels started hitting the market in 2005 and have become more prevalent with each new year. Today, there are many ways to make your own solar panels, from putting together a solar panel kit to planning a solar array.

2015: Flexible Printed Solar Panels Hit the Market. Solar cells as thin as paper can now be manufactured using an industrial printer. They have 20% power conversion efficiency, and a single strip can produce up to 50 watts per square meter. This is great news for the 1.3 billion people in developing countries, as the strips are flexible and inexpensive to produce.

2016: Sunless Solar Power Is Discovered. A research team from the University of California, Berkeley, and the Australian National University discovered new properties of

nanomaterial. One of these properties is called magnetic hyperbolic dispersion, which means the material glows when heated. If combined with thermos photovoltaic cells, it could turn heat into electricity without the need for sunlight.

Solar power has come a long way in the past 200 years, from observing the properties of light to finding new ways to convert it into power. This technology shows no signs of slowing down if anything, it is advancing at an unprecedented rate. Stay up to date on the latest solar news and advances to decide if solar power is right for you[5].

1.3 Introduction to Perovskites

Perovskite solar cells are kind of solar cell device which use perovskite based material as the light absorbing layer**.** For the first time in 2009, the inorganic-organic hybrid perovskite materials were applied in liquid dye-sensitized solar cells. In 2013, the power conversion efficiency successfully reached 15%, followed by great amount of research papers bursting out. Till 2017, the highest efficiency is certified to 22.1%, and the reported efficiency is even up to 27.3%. They quickly go beyond dye-sensitized solar cells and organic solar cells. It is expected the perovskite has its efficiency same to the single-crystal silicon cells. The "game changer" of solar cells is coming. The perovskite solar cells are cheap and easily to be made, which will benefit both science and industry. This review summarized recent development of both perovskite materials and solar cell devices, not only including new material developments of perovskite compositions, structures, and fabrication methods, but also focusing on device structures, charge transfer mechanism and stability properties of perovskite solar cells. Their perspective is also estimated [6].

Metal halide perovskites possess unique features that make them exciting for solar cell applications. The raw materials used, and the possible fabrication methods (such as various

printing techniques) are both low cost [7]. Their high absorption coefficient enables ultrathin films of around 500 nm to absorb the complete visible solar spectrum. These features combined result in the possibility to create low cost, high efficiency, thin, lightweight and flexible solar modules. In July2015 major hurdles were that the largest perovskite solar cell was only the size of a fingernail and that they degraded quickly in moist environments. However, a work published in June 2017 successfully demonstrated large scale perovskite solar modules with no observed degradation over one year [8]. Perovskite solar cell bandgaps are tunable and can be optimized for the solar spectrum by altering the halide content in the film (i.e., by mixing I and Br). The Shockley–Queisser limit radiative efficiency limit, also known as the detailed balance limit, is about 31% under an AM1.5G solar spectrum at 1000W/m^2, for a Perovskite bandgap of 1.55 eV [9]. This is slightly smaller than the radiative limit of gallium arsenide of bandgap 1.42 eV which can reach a radiative efficiency of 33%. Values of the detailed balance limit are available in tabulated form and a MATLAB program for implementing the detailed balance model has been written. In the meantime, the drift-diffusion model has been found to successfully predict the efficiency limit of perovskite solar cells. There are two prerequisites for predicting and approaching the perovskite efficiency limit. First, the intrinsic radiative recombination needs to be corrected after adopting optical designs which will significantly affect the open-circuit voltage at its Shockley–Queisser limit. Second, the contact characteristics of the electrodes need to be carefully engineered to eliminate the charge accumulation and surface recombination at the electrodes. With the two procedures, the accurate prediction of efficiency limit and precise evaluation of efficiency degradation for perovskite solar cells are attainable by the drift-diffusion model [10].

Perovskite is possible to apply to flexible and semitransparent solar cells due to the low fabrication temperature, which have been widely explored in the Dye Synthesized Solar Cell (DSSC) and Organic Photovoltaics (OPV) field [11]. Now the cell is pacing to its commercialization. There still remain questions. Its microscopic mechanism is not fully understood at this moment, which needs to be further studied systematically. One of the top issues in its commercialization is environmental safety. Solar energy is regarded as clean energy and environmentally safe. Pb element is widely used in solar cells, which will generate large scale heavy metal pollution. This should be avoided by any means. However, though some cells are produced without or lower Pb element ratio, their efficiencies drop dramatically. This makes the unleaded cells away from applications [12]. The high efficient perovskite solar cell without Pb is an important topic for exploration. Another key issue is the stability of perovskite, which is also important to its real application. There are limited studies on this issue. With the cell efficiency being near to its top power conversion efficiency in theory, the study on cell stability will take the main position towards commercialization. The stability of the perovskite cell is easily affected by its surrounding atmosphere. Optimizing the material and structure of devices will benefit its real application finally. Overall, high efficiency perovskite photovoltaic devices provide a brilliant new route for thin-film solar cells. Highly stable, high efficient light conversion devices are just at near future [13].

Recent advances in organic-inorganic hybrid perovskite solar cells (PSCs) with methyl ammonium lead iodide as the archetypal material, have led to the advent of new low cost photovoltaic (PV) technology that could be a viable competitor to the commercially available Silicon based solar cells [14]. Apart from low cost, simple device processing and manufacturability combined compatibility with roll-to-roll processing and fabrication on

flexible substrates add to the merits of the perovskite PV technology. The term "perovskite" was attributed to the crystal structure of calcium titanate ($CaTiO_3$), which was discovered by the German mineralogist Gustav Rose in 1839 and named in honor of the Russian mineralogist Lev Perovski. The organic–inorganic hybrid halide based perovskites are widely studied in the 1990s for the application in transistor technology and light emitting diodes, due to their excellent opto-electronic properties and solution processability of these materials [15]. Organic–inorganic hybrid halide based perovskites are a group of materials with the general formula ABX_3, where A is an organic cation ($CH_3NH_3^+$ or $NH_2CH_3NH_2^+$), B is a divalent cation (Pb^{2+} or Sn^{2+}) and X is a monovalent halide anion (I^-, Br^-, or Cl^-) [16]. Organic-inorganic hybrid halide based perovskites was first used in photovoltaics as a sensitizer replacing the dye pigment in Dye sensitized solar cells (DSSCs), which reported a 3.8% PCE in 2009. The devices employed liquid electrolyte as hole transporting layer (HTL), therefore gained little attention due to low efficiency and poor stability. Later, the liquid electrolyte was replaced by solid-state HTL (Spiro-OMeTAD), which resulted in a solid-state device with relatively high efficiency, ~9%, in 2012. This breakthrough led to the so-called "perovskite fever" [17] attracting much research much research interest in the following years, eventually increasing the efficiency to a record 22.1% in early 2016. The trend in increase of performance efficiency of perovskite solar cells along with the associated timeline is shown in Figure 2.3 and the corresponding device details are depicted in Table 1.

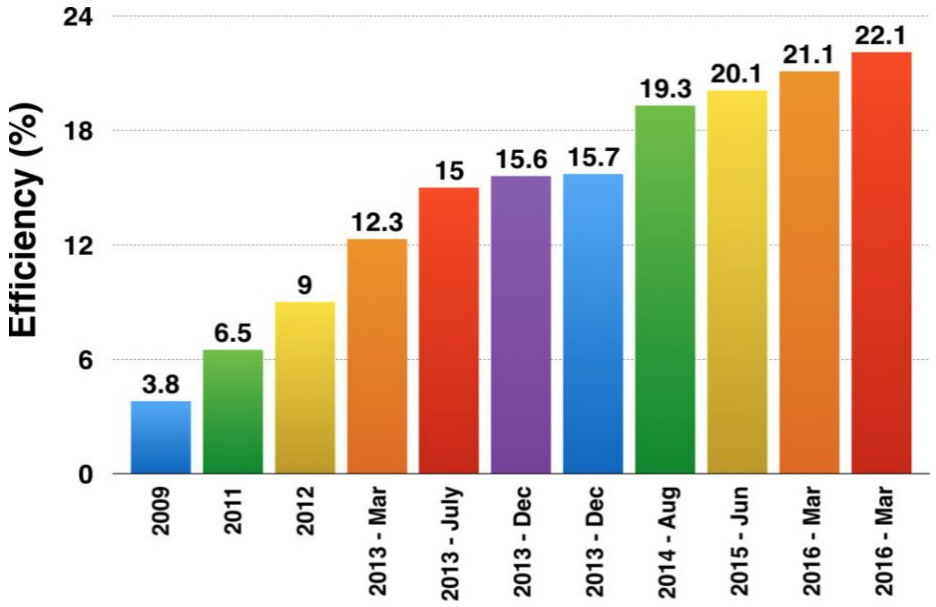

Figure 1.1 Annual increase in efficiency of perovskite solar cells.

Table 1.1 Development trend in perovskite solar cells with details of device structure.

Year	Device Structure	PCE (%)	Reference
2009	**FTO/bl-TiO_2/mp-TiO_2/$CH_3NH_3PbI_3$/Redox Liquid electrolyte/Pt**	**3.8**	**[16]**
2011	**FTO/bl-TiO_2/mp-TiO_2/$CH_3NH_3PbI_3$/ Redox Liquid electrolyte/Pt**	**6.5**	[18]
2012	**FTO/bl-TiO_2/mp-TiO_2/$CH_3NH_3PbI_3$/ Spiro-OMeTAD/Au**	**9**	[19]
Mar 2013	**FTO/bl-TiO_2/mp-Al_2O_3/ $CH_3NH_3PbI_{3-x}Cl_x$/Spiro-OMeTAD/Ag**	**12.3**	[20]
July 2013	**FTO/bl-TiO_2/mp-TiO_2/$CH_3NH_3PbI_3$/ Spiro-OMeTAD/Au**	**15**	[21]

Year	Device Structure	PCE(%)	Reference
2013	FTO/Graphene-TiO_2/mp-Al_2O_3/ $CH_3NH_3PbI_{3-x}Cl_x$/OMeTAD/Au	15.6	[22]
Dec 2013	ITO/np-ZnO/$CH_3NH_3PbI_3$/ Spiro-OMeTAD/Ag	15.7	[23]
August 2014	ITO-PEIE/Y-TiO_2/$CH_3NH_3PbI_{3-x}Cl_x$/ Spiro-OMeTAD/Au	19.3	[24]
June 2015	FTO/bl-TiO_2/mp-TiO_2/$(FAPbI_3)1–x(MAPbBr_3)$ *x*/ PTAA/Au	20.1	[25]
Mar 2016	FTO/bl-TiO_2/mp-TiO_2/$Cs_x(MA_{0.17}FA_{0.83})_{(1-x)}$ $Pb(I_{0.83}Br_{0.17})_3$/Spiro-OMeTAD	21.1	[26]
Mar2016	N/A	22.1	[27]

The stride of progress has been extraordinary and unprecedented in PV history and can be ascribed to numerous factors related to inexpensive fabrication costs, ease of processing, and the excellent electronic and optical properties of the perovskite materials. Moreover, the superior performance of the PSCs is reflected in their high open circuit voltage (Voc). The solar cell device efficiency (η) is generally defined as _ = Jsc (short circuit current density) _

Voc (open circuit voltage) _ FF (fill factor). According to detailed balance theory, the maximum open circuit voltage (Voc-max) of a semiconductor absorber is approximately its bandgap energy (Eg) subtracted/reduced by 0.25 eV and the ratio of Voc-max/Eg indicates the efficacy of the semiconductor material as a solar cell absorber. In line with this, the maximum theoretical limit (SQ-limit) calculated for the perovskite solar cells employing CH3NH3PbI3-xClx absorber (Eg ~1.55 eV) is as follows: Jsc(SQ-limit) is 27.20 (mA/cm2), Voc(SQ-limit) is 1.28 V, FF(SQ-limit) is 90.2 and PCE(SQ-limit) is 31.4%. It clearly indicates that perovskite solar cells have immense potential for further development and the progress is promising.

1.3 Motivation

The perovskite solar cells are the new kind of solar cells which have a rapid increase in PCE's from 3.8% in 2009 to 22.1% in 2016 owing to low cost, good stability, and easy fabrication process, motivated me to do research in perovskite solar cells. Also need to carry out simulation using freely available, popular and efficient solar cell simulator for the purpose of investigating ways to enhance performance of perovskite solar cell.

1.4 Objectives

The main goal of this project is to explore new architecture for perovskite solar cell with high efficiency. Using perovskite in a solar cell is an emerging technology which enhances the efficiency greater than the traditional silicon solar cell. To accomplish this goal the specific objectives are to:

i) It involves in selection of a suitable materials which fits the properties of electron Transport layer (ETL), Hole Transport Layer (HTL) and absorber layer.

ii) Using these materials to make a theoretical perovskite solar cell. Thereafter simulate this whole cell architecture using wxAmps solar cell simulation software to get hopeful performance results.

iii) Theoretically study the effect of each layer of perovskite solar cell on performance.

iv) Analyze and compare the results overall performance in between different architectures that give the best results to find out the best performing solar cell.

1.5 Organization of Thesis

Chapter 1: Includes background of solar energy, history of solar cells and its evolution and introduction to perovskite solar cells.

Chapter 2: It is about the theory of solar cells which includes working principles and fabrication methods.

Chapter 3: It is mainly about the simulation software "WxAmps" includes its working principle and input parameters are explained.

Chapter 4: This chapter is mainly about the simulation results and analysis of perovskite solar cell.

Chapter 5: This chapter explains about the summary and future work.

CHAPTER 2

THEORY

2.1 Introduction to solar cell device

Energy from the sun comes to Earth in tiny pieces called photons. Photons can hit atoms and give off energy. This is why your skin feels warm when you stand in sunlight: photons have traveled all the way from the Sun and are hitting the atoms in your skin to produce heat. Since they produce electricity from light, solar cells are also called photovoltaic cells ("photo" is Greek for light and "volt" is a unit of electricity). A photovoltaic cell works by capturing a photon from the sun using special metals called semiconductors. When photons hit semiconductors, they can produce electricity instead of heat. By using semiconductors to build solar cells, we can produce electricity from sunlight. Silicon, like the silicon found in a computer chip, is a common semiconductor in a photovoltaic cell. When a photon hits silicon, it will sometimes release an electron. The solar cell traps all the electrons released by the silicon and pushes them in one direction, which creates an electric current. Solar cells are used on spaceships like the International Space Station pictured below, but are also used on Earth in places that get lots of sunlight throughout the year. The more sunlight they receive, the more electricity they produce, so areas that don't get much sun aren't good places for using solar cells [27]. The external structure of the solar cell device is shown in figure 2.1.

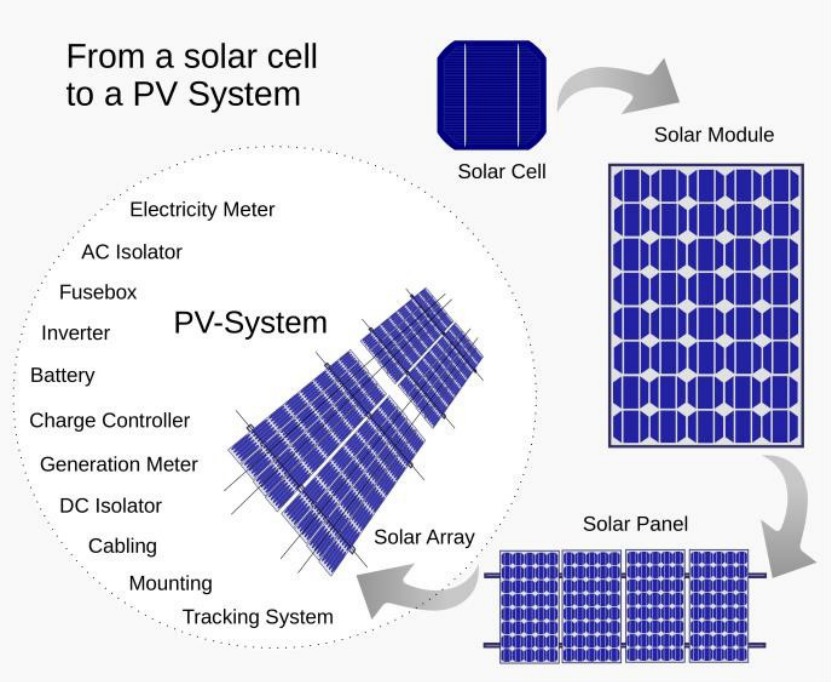

Figure 2.1. From a solar cell to PV system[27]

The internal structure of the device is shown in the Figure 2.1 which introduce the working principles of the solar cell-light inducing into the active layer, holes and electrons generating and then transferring through the transporting layer and finally gathering at the electrode, forming the photo current.

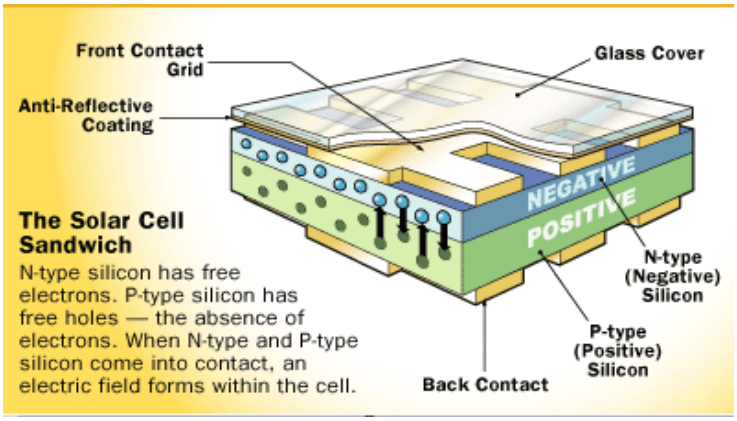

Figure 2.2 Working principles of solar cell device [28]

The collection of light-generated carriers does not by itself give rise to power generation. In order to generate power, a voltage must be generated as well as a current. Voltage is generated in a solar cell by a process known as the "photovoltaic effect". The collection of light-generated carriers by the *p*-*n* junction causes a movement of electrons to the *n*-type side and holes to the *p*-type side of the junction. Under short circuit conditions, there is no buildup of charge, as the carriers exit the device as light-generated current.

However, if the light-generated carriers are prevented from leaving the solar cell, then the collection of light-generated carriers causes an increase in the number of electrons on the *n*-type side of the *p*-*n* junction and a similar increase in holes in the *p*-type material. This separation of charge creates an electric field at the junction which is in opposition to that already existing at the junction, thereby reducing the net electric field. Since the electric field represents a barrier to the flow of the forward bias diffusion current, the reduction of the electric field increases the diffusion current. A new equilibrium is reached in which a voltage exists across the *p*-*n* junction. The current from the solar cell is the difference between I_L and the forward bias current. Under open circuit conditions, the forward bias of the junction increases to a point where the light-generated current is exactly balanced by the forward bias diffusion current, and the net current is zero. The voltage required to cause these two currents to balance is called the "open-circuit voltage". The following animation shows the carrier flows at short-circuit and open-circuit conditions.

2.2 Working Principle of Typical Silicon(Si) Solar Cell

A solar cell is an electronic device which directly converts sunlight into electricity. Light shining on the solar cell produces both a current and a voltage to generate electric power. This process requires firstly, a material in which the absorption of light raises an electron to a higher energy state, and secondly, the movement of this higher energy electron from the solar cell into an external circuit. The electron then dissipates its energy in the external circuit and returns to the solar cell. A variety of materials and processes can potentially satisfy the requirements for photovoltaic energy conversion, but in practice nearly all photovoltaic energy conversion uses semiconductor materials in the form of a *p*-*n* junction.

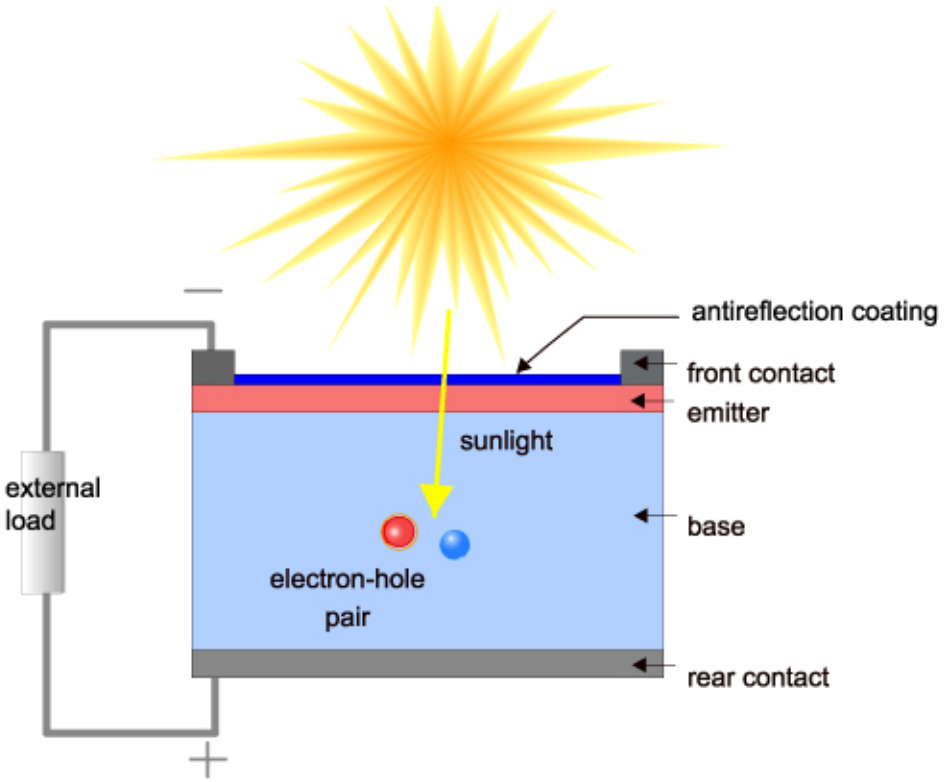

Figure 2.3 Cross section of a Solar cell[28]

The basic steps in the operation of a solar cell are:

- The generation of light-generated carriers;
- The collection of the light-generated carries to generate a current;
- The generation of a large voltage across the solar cell; and
- The dissipation of power in the load and in parasitic resistances.

The generation of current in a solar cell, known as the "light-generated current", involves two key processes. The first process is the absorption of incident photons to create electron-hole pairs. Electron-hole pairs will be generated in the solar cell provided that the incident photon has an energy greater than that of the band gap. However, electrons (in the *p*-type material), and holes (in the *n*-type material) are meta-stable and will only exist, on average, for a length of time equal to the minority carrier lifetime before they recombine. If the carrier recombines, then the light-generated electron-hole pair is lost and no current or power can be generated. A second process, the collection of these carriers by the *p-n* junction, prevents this recombination by using a *p-n* junction to spatially separate the electron and the hole. The carriers are separated by the action of the electric field existing at the *p-n* junction. If the light-generated minority carrier reaches the *p-n* junction, it is swept across the junction by the electric field at the junction, where it is now a majority carrier. If the emitter and base of the solar cell are connected (i.e., if the solar cell is short-circuited), the light-generated carriers flow through the external circuit. The collection of light-generated carriers does not by itself give rise to power generation. In order to generate power, a voltage must be generated as well as a current. Voltage is generated in a solar cell by a process known as the "photovoltaic effect". The collection of light-generated carriers by the *p-n* junction causes a movement of

electrons to the *n*-type side and holes to the *p*-type side of the junction. Under short circuit conditions, there is no buildup of charge, as the carriers exit the device as light-generated current. However, if the light-generated carriers are prevented from leaving the solar cell, then the collection of light-generated carriers causes an increase in the number of electrons on the *n*-type side of the *p*-*n* junction and a similar increase in holes in the *p*-type material. This separation of charge creates an electric field at the junction which is in opposition to that already existing at the junction, thereby reducing the net electric field. Since the electric field represents a barrier to the flow of the forward bias diffusion current, the reduction of the electric field increases the diffusion current. A new equilibrium is reached in which a voltage exists across the *p*-*n* junction. The current from the solar cell is the difference between I_L and the forward bias current. Under open circuit conditions, the forward bias of the junction increases to a point where the light-generated current is exactly balanced by the forward bias diffusion current, and the net current is zero. The voltage required to cause these two currents to balance is called the "open-circuit voltage" [28].

2.3 Solar Cell Parameters

(i) IV Curve

The IV curve of a solar cell is the superposition of the IV curve of the solar cell diode in the dark with the light-generated current. The light has the effect of shifting the IV curve down into the fourth quadrant where power can be extracted from the diode. Illuminating a cell adds to the normal "dark" currents in the diode so that the diode law becomes:

$$I = I_0 \left[\exp\left(\frac{qV}{nkT}\right) - 1 \right] - I_L \tag{2.1}$$

(ii) Short Circuit Current (I_{sc})

The short-circuit current is the current through the solar cell when the voltage across the solar cell is zero (i.e., when the solar cell is short circuited). Usually written as I_{SC}, the short-circuit current is shown on the IV curve below.

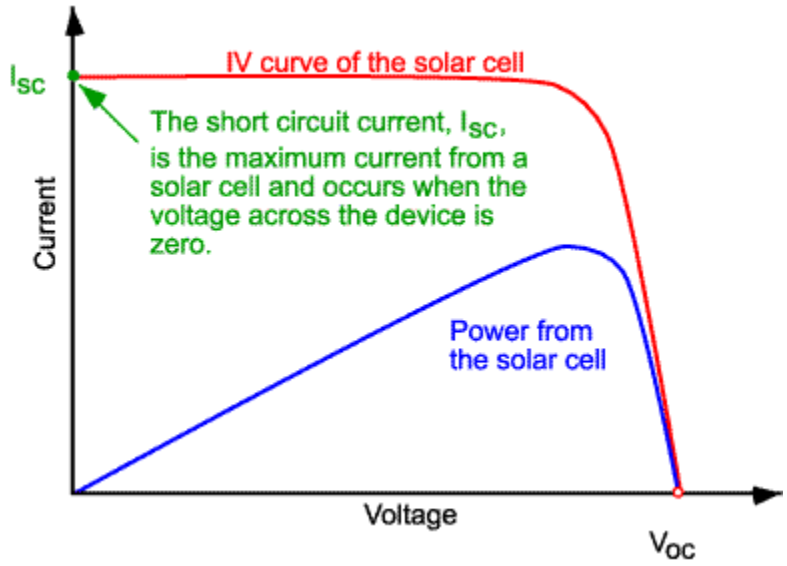

Figure 2.4 IV curve of a solar cell showing short-circuit current [28].

The short-circuit current is due to the generation and collection of light-generated carriers. For an ideal solar cell at most moderate resistive loss mechanisms, the short-circuit current and the light-generated current are identical. Therefore, the short-circuit current is the largest current which may be drawn from the solar cell.

The short-circuit current depends on a number of factors which are described below:

- **The area of the solar cell.** To remove the dependence of the solar cell area, it is more common to list the short-circuit current **density** (J_{sc} in mA/cm^2) rather than the short-circuit current;
- **The number of photons** (i.e., the power of the incident light source). Isc from a solar cell is directly dependent on the light intensity as discussed in Effect of Light Intensity;
- **The spectrum of the incident light.** For most solar cell measurement, the spectrum is standardized to the AM1.5 spectrum;
- **The optical properties** (absorption and reflection) of the solar cell (discussed in Optical Losses); and
- **The collection probability** of the solar cell, which depends chiefly on the surface passivation and the minority carrier lifetime in the base.

When comparing solar cells of the same material type, the most critical material parameter is the diffusion length and surface passivation. In a cell with perfectly passivated surface and uniform generation, the equation for the short-circuit current can be approximated as:

$$J_{SC} = qG\left(L_n + L_p\right) \tag{2.2}$$

where G is the generation rate, and L_n and L_p are the electron and hole diffusion lengths respectively. Although this equation makes several assumptions which are not true for the conditions encountered in most solar cells, the above equation nevertheless indicates that the short-circuit current depends strongly on the generation rate and the diffusion length. Silicon solar cells under an AM1.5 spectrum have a maximum possible current of 46 mA/cm^2. Laboratory devices have measured short-circuit currents of over 42 mA/cm^2, and commercial solar cell have short-circuit currents between about 28 mA/cm^2 and 35 mA/cm^2.

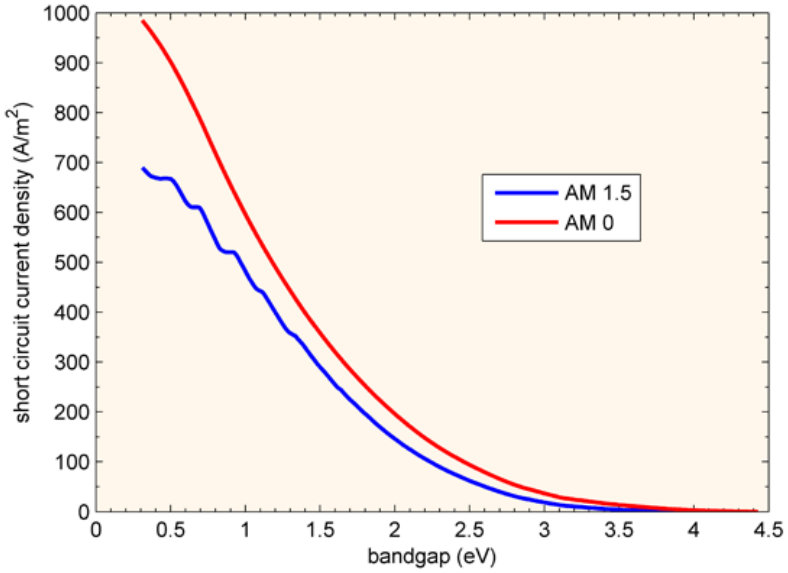

Figure 2.5 Bandgap vs Short circuit current density property of a solar cell [28].

(iii) Open-Circuit Voltage (V_{oc})

The open-circuit voltage, V_{OC}, is the maximum voltage available from a solar cell, and this occurs at zero current. The open-circuit voltage corresponds to the amount of forward bias on the solar cell due to the bias of the solar cell junction with the light-generated current. The open-circuit voltage is shown on the IV curve below (Fig 2.6).

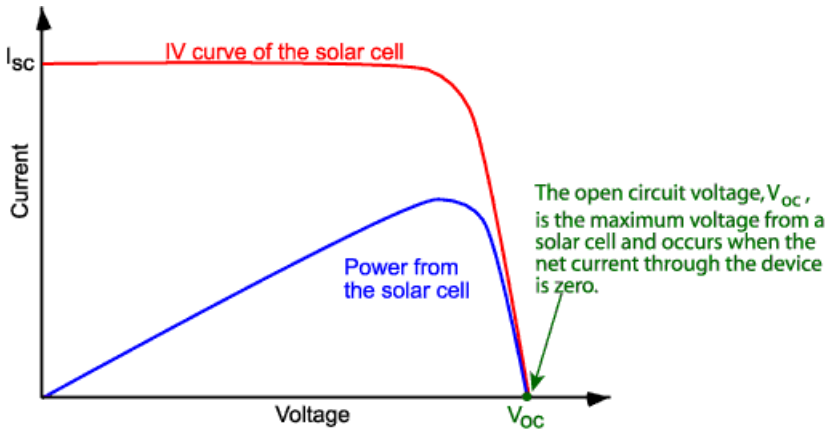

Figure 2.6 IV curve of a solar cell showing the open-circuit voltage [28].

- An equation for V_{oc} is found by setting the net current equal to zero in the solar cell equation to give:

$$V_{OC} = \frac{nkT}{q} \ln\left(\frac{I_L}{I_0} + 1\right) \tag{2.3}$$

(iv) Fill Factor (FF)

The short-circuit current and the open-circuit voltage are the maximum current and voltage respectively from a solar cell. However, at both of these operating points, the power from the solar cell is zero. The "fill factor", more commonly known by its abbreviation "FF", is a parameter which, in conjunction with V_{oc} and I_{sc}, determines the maximum power from a solar cell. The FF is defined as the ratio of the maximum power from the solar cell to the product of V_{oc} and I_{sc}. Graphically, the FF is a measure of the "squareness" of the solar cell and is also the area of the largest rectangle which will fit in the IV curve. The FF is illustrated below.

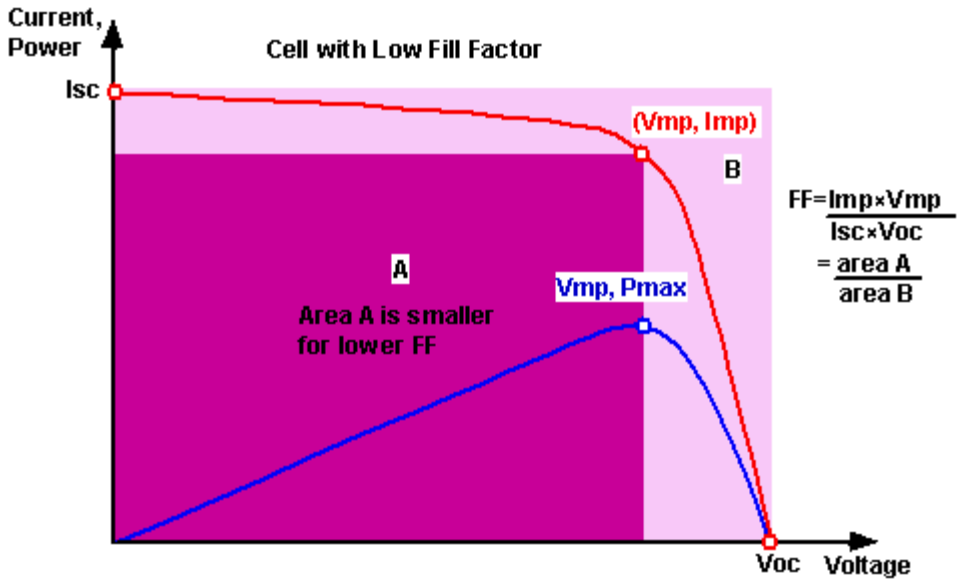

Figure 2.7 Graph of cell output current (red line) and power (blue line) as function of voltage. Also shown are the cell short-circuit current (I_{sc}) and open-circuit voltage (V_{oc}) points, as well as the maximum power point (V_{mp}, I_{mp}) [28].

(v) Efficiency (η)

The efficiency is the most commonly used parameter to compare the performance of one solar cell to another. Efficiency is defined as the ratio of energy output from the solar cell to input energy from the sun. In addition to reflecting the performance of the solar cell itself, the efficiency depends on the spectrum and intensity of the incident sunlight and the temperature of the solar cell. Therefore, conditions under which efficiency is measured must be carefully controlled in order to compare the performance of one device to another. Terrestrial solar cells are measured under AM1.5 conditions and at a temperature of 25°C. Solar cells intended for space use are measured under AM0 conditions.

The efficiency of a solar cell is determined as the fraction of incident power which is converted to electricity and is defined as:

$$P_{max} = V_{OC} I_{SC} FF \tag{2.4}$$

$$\eta = \frac{V_{OC} I_{SC} FF}{P_{in}} \tag{2.5}$$

Where:

V_{oc} is the open-circuit voltage;

I_{sc} is the short-circuit current;

FF is the fill factor and

η is the efficiency.

2.4 Perovskite Crystal Structure

The crystal structure of perovskites (ABX_3), typically consists of a unit cell with five atoms in a cubic structure (α phase), in which the cation A has twelve nearest neighboring anions X and the cation B has six as shown in Figure 2.4(a). Under ideal conditions, in order to maintain high-symmetry cubic structure, the tolerance factor t should be close to 1. The tolerance factor t is expressed as a function of ionic radii of A, B and X site ions, which is written as

$$t = \frac{(R_A + R_X)}{\left\{\sqrt{2}(R_B + R_X)\right\}} \tag{2.6}$$

where R_A, R_B, and R_X are the ionic radii of the corresponding ions. Larger the deviation from the ideal value t, the crystal structure will be distorted and the symmetry would be lowered.

Therefore, in order to satisfy the ideal tolerance factor ($t \approx 1$), the A-site ion must be much larger than the B-site ion. In the case of halide perovskites, in general, large Pb or Sn atom occupies the B site; hence the cation at A-site must be extremely large. At finite temperature, cubic structure may exist when t lies between 0.89 and 1, and smaller t (i.e., $t < 0.89$) could result in lower-symmetry tetragonal (β phase) or orthorhombic (γ phase) crystal structures. On the other hand, larger t (i.e., $t > 1$), could undermine the three-dimensional (3D) B–X network, leading to a two-dimensional (2D) layer structure. It is noteworthy to mention that the DFT calculations computed at zero temperature have revealed that the orthorhombic (γ phase) is the most stable and the cubic (α phase) is the most unstable structure, since it is very difficult to satisfy the ideal condition $t = 1$. However, transitions between those crystal structures often occur in most perovskites at finite temperature. The tolerance factors of some of the notable hybrid perovskite materials are shown in Figure 2.4(c). The perovskite material ($CH_3NH_3PbI_3$) undergoes reversible phase transition as a function of temperature. At low temperature of about 100 K, a stabilized orthorhombic (γ) phase exists and the phase transition between the tetragonal (β) phase and orthorhombic (γ) phase occurs at around 160 K. The crystal structure for three phases is shown in Figure 2a–c. The tetragonal-cubic phase transition partially influences the thermal stability issue for $MAPbI_3$ based PSCs. In the case of formamidinium iodide ($HC(NH_2)_2PbI_3$) based perovskites, a similar phase transition occurs at higher temperature, hence it is relatively stable compared to $MAPbI_3$. A recent report revealed light soaking could also induce reversible structure transformation in halide perovskite materials [29].

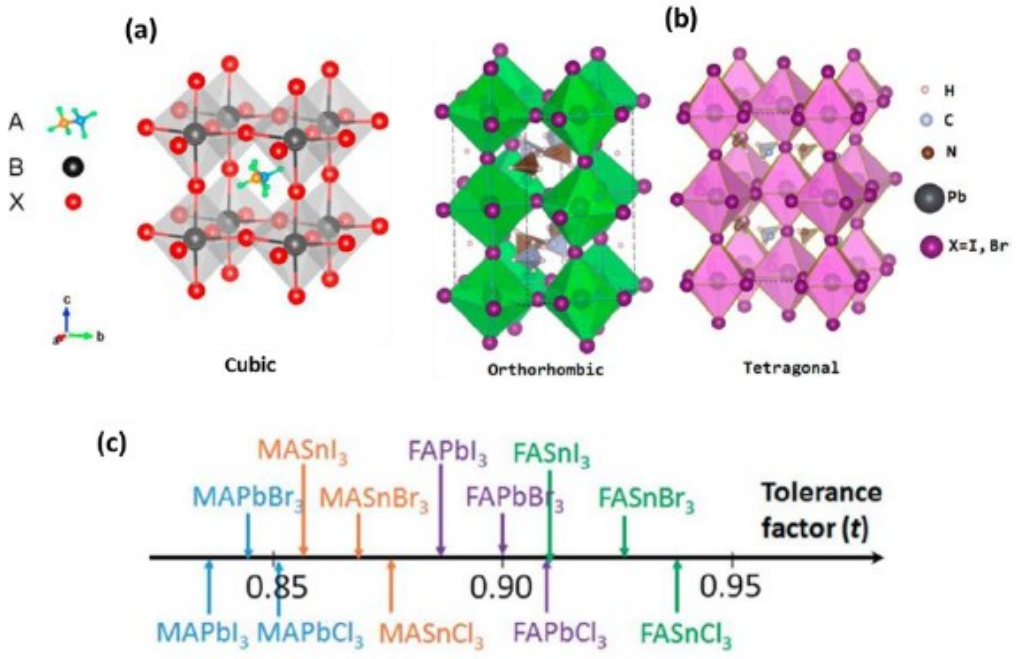

Figure 2.8 (a) Crystal structure of cubic (α phase); (b) Crystal structure of the tetragonal crystal system (β) phase and orthorhombic (γ) phase of $MAPbX_3$; and (c) the tolerance factor for different perovskite material systems, t=1 is ideal.

Image: (a) [27]; (b) [28]; (c) [29].

2.5 Electronic Structure of Perovskites

The electronic structure of hybrid perovskites especially near the band edge is predominantly dictated by the BX_6 (octahedra) building blocks. For instance, in the case of $[PbI_6]4^-$ units in particular, the valence band (or highest occupied molecular orbital, HOMO) is determined by the Pb 6s–I 5p σ-antibonding orbital. Similarly, the conduction band (or lowest unoccupied molecular orbital, LUMO) is determined by the Pb 6p–I 5p π-antibonding and Pb 6p–I 5s σ-antibonding orbitals. The unusual electronic properties of hybrid perovskites are mainly ascribed to the lone pair of s electrons in Pb cation, i.e., unlike most cations whose

outer s orbitals are empty, Pb has an occupied 6s orbital, which lies below the top of the valence bands [31]. The valence band maximum (VBM) has strong Pb s and I p antibonding character, whereas the conduction band minimum (CBM) is mostly contributed from the Pb p state, which attributes to the unique dual nature (ionic and covalent characteristics) of electronic structures in halide perovskites. Figure 2.5 (top) shows the atomic structure of perovskite (ABX_3) and the contribution of each of its atoms/ions towards the electronic structure of the perovskite material. In the hybrid perovskite structure of $MAPbI_3$, the iodine ions at the X-site forms the valence band and the lead (anion) at the B-site forms the conduction band, while organic cation at the A-site remains electronically inactive but contributes to the structural stability and tolerance factor of the perovskite structure. The contributions of MA, Pb, and I on the density of state of $MAPbI_3$ perovskite are shown in Figure 2.5 (bottom). It can be clearly seen that the grey colored distribution pertaining to the A cation lies well below the valence band maximum (VBM), therefore does not contribute to the bandgap electronically.

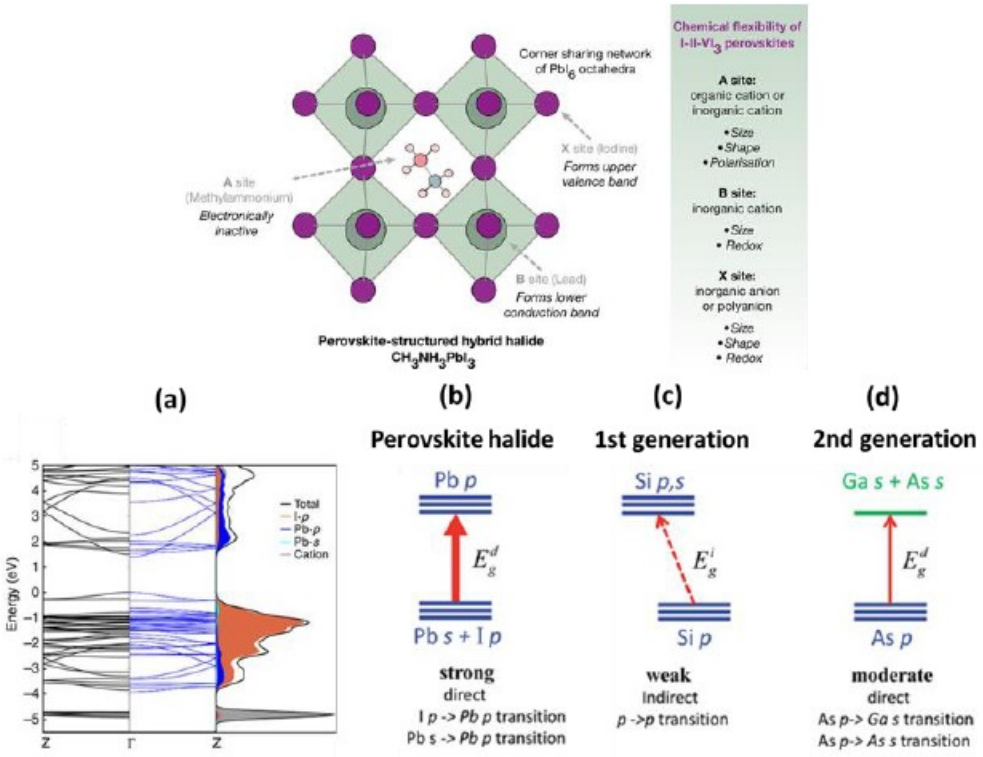

Figure 2.9 Top: Schematic of the perovskite crystal structure with respect to the A, B and X lattice sites and their contribution to the electronic structure [34]; **Bottom:** (**a**) Contributions of MA, Pb, and I on the density of state of $MAPbI_3$ perovskite[35]. The schematic optical absorption of: (**b**) halide perovskite solar cell absorber; (**c**) first-generation (Si); and (**d**) second-generation (GaAs as example)[36].

2.6 Working Principle of a Perovskite Solar Cell

Solar cells are usually composed of an N-type semiconductor and a P-type semiconductor. When the solar light is shining on the active layer in the solar cell, it can produce two excitons-electrons and holes. Then the electrons with negative charge transport through the N-type semiconductors (also called acceptor) finally gather around the cathode while the holes with positive charge transport through the P-type

semiconductor (also called donor) finally gather around the anode. When you apply load in the external circuit, there will be current flows between the cathode and the anode. This is how photocurrent generates. Figure 2.6 is a rough description of the generation of photocurrent.

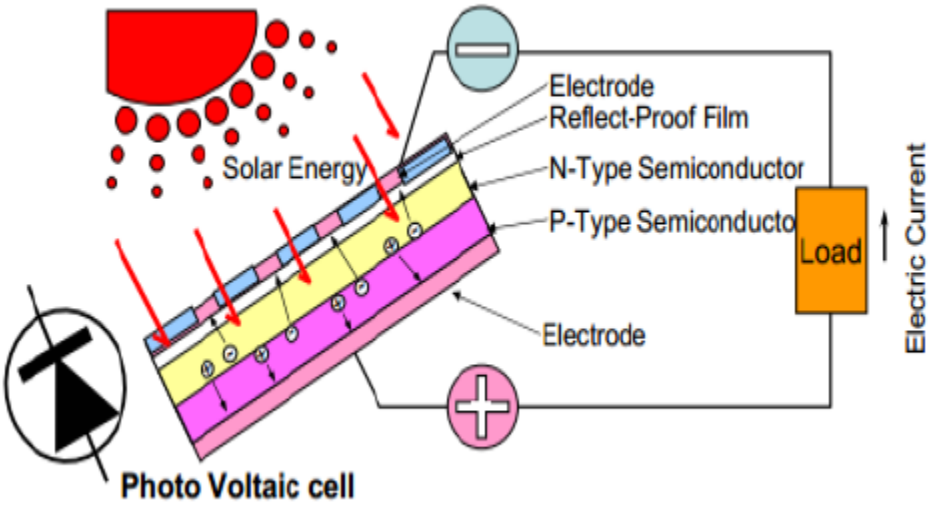

Figure 2.10 Basic Working Mechanisms of solar cell device [37].

Traditional silicon solar cell has limited development prospect due to its high cost in the silicon refining processing and pollution issue. Meanwhile, polymer solar cells, which comes to another option for the solar cell device, does not have the very high device performance. In recent years, the methyl ammonium lead halide perovskite ($CH_3NH_3PbI_3$) materials have emerged as promising candidates due to their excellent optical and electrical properties such as the large light absorption coefficient (5.7×104 cm^{-1} at 600 nm), high charge carrier mobility

(hole mobility of 164 cm^2 V^{-1} S^{-1} and electron mobility of 24 $cm^2V^{-1}S^{-1}$ for $CH_3NH_3PbI_3$ single-crystal perovskite), long charge diffusion length (~100nm), easy fabricating procedure (solution-processing) etc. The following figures show the basic working mechanism of the perovskite layer and the development of perovskite solar cells compared to other type solar cells. The role that perovskite layer play in the total device structure is functioning as the active layer (also called light absorbing layer) (see Figure 2.7). Charge carriers then transport through hole transfer layer (HTL) and electron transfer layer (ETL), gather at the corresponding electrode, form the photocurrent. That is how perovskite solar cells work. As for the device performance, from Figure 2.8 we can see, although perovskite solar cells have been researched for only a few years, the efficiency has a huge improving which indicate that perovskite will be a very prospect material in photovoltaic field.

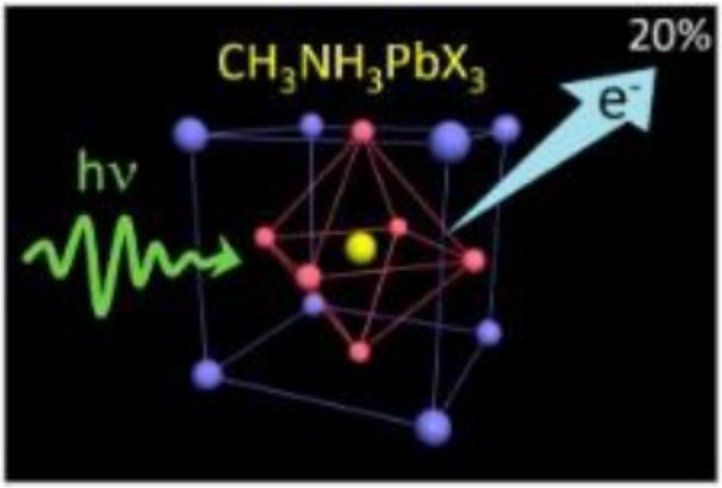

Figure 2.11 Working Mechanism of Perovskite Solar Cell [37]

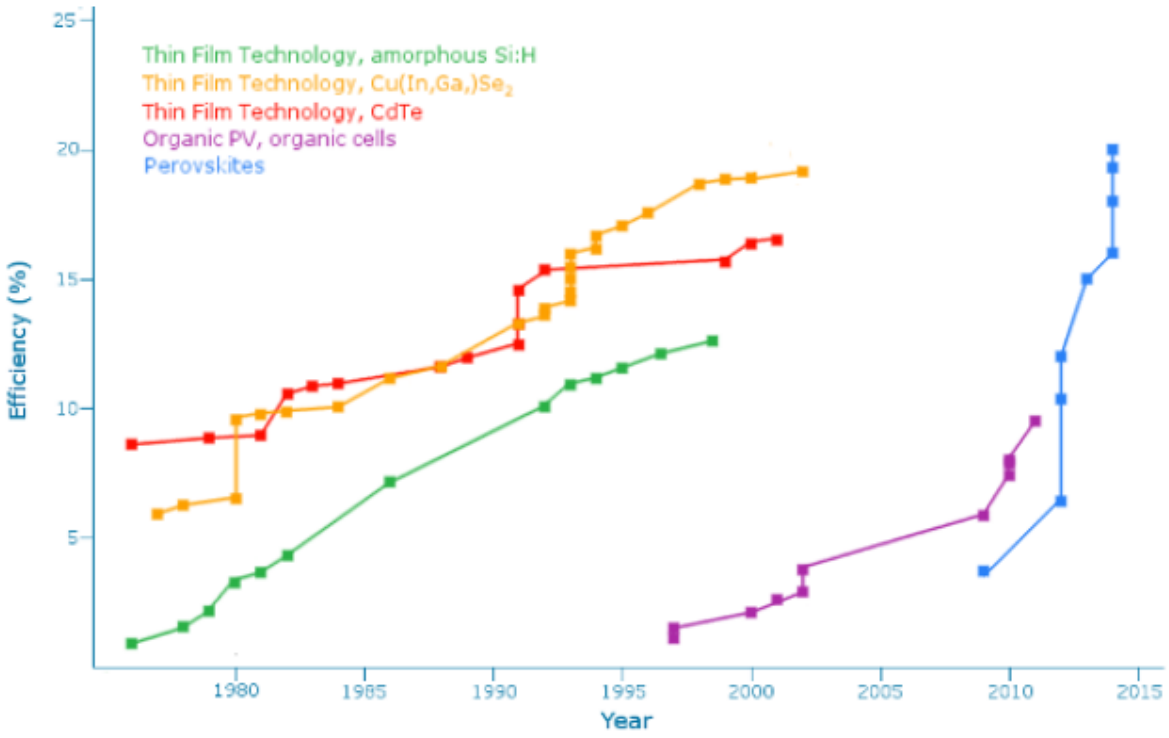

Figure 2.12 Device Efficiency Development [37]

2.7 Perovskite Solar Cell Device Architectures

Perovskite solar cells evolved from the mesoscopic structure (Figure 2.9a) in which the halide perovskite semiconductors replaced the light harvesting dye. Later, the liquid electrolyte was replaced with a solid-state hole conductor. The advent attracted much interest in the PV community, which resulted in the development of other device structures as shown in Figure 2.6b–d. The planar device structure is developed in which the perovskite absorber is sandwiched between the electron (ETM) and hole transporting materials (HTM). The n-i-p is also called as normal device structure and p-i-n structure is also called as inverted device structure. Simply, depending on the position of the ETM and HTM, the device structure varies

[28]. The details about the different electron and hole transporting layers are discussed in the forthcoming section.

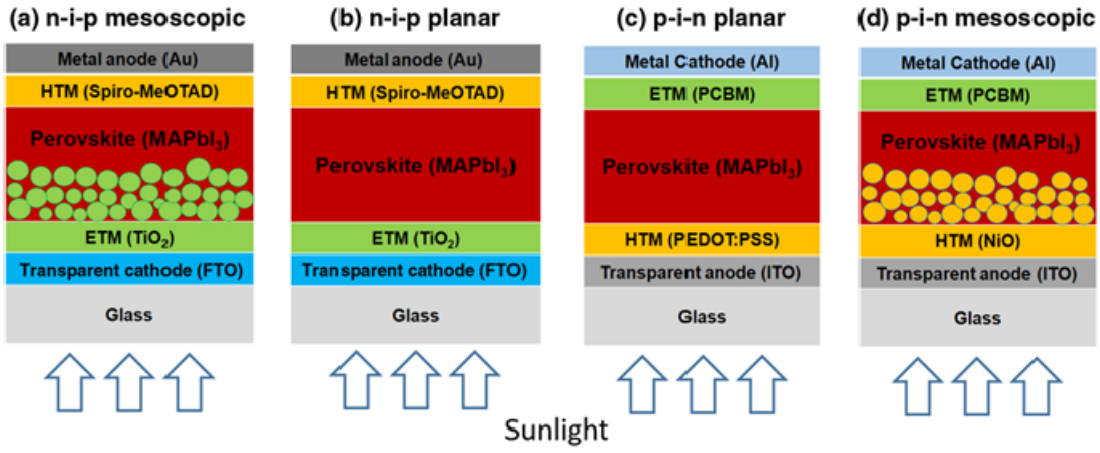

Figure 2.13 Schematic diagrams of perovskite solar cells in the: (a) n-i-p mesoscopic; (b) n-i-p planar;

(c) p-i-n planar; and (d) p-i-n mesoscopic structures. (a, b) Normal device structure; and (c, d) inverted device structure [37].

Recently, demonstrated perovskite solar cells with fullerene as electron transporting layer (ETL) which exhibited PCE >10% in n-i-p planar device configuration[37]. The authors incorporated an innovative fullerene-saturation approach/strategy (the perovskite processing solution is saturated with fullerene) to avoid the damage of the fullerene film through dissolution during the deposition of the perovskite layer. Another interesting finding was also demonstrated by the same research group, where the perovskite solar cells are fabricated without the electron transport layer with solution processed methylammonium lead triiodide perovskite–C70 fullerene ($MAPbI_3$:C70) blend films on fluorine-doped tin oxide (FTO)-coated glass substrates. The ETL-free devices thus fabricated exhibited PCE of 13.6% with

significantly low carrier recombination when compared to conventional $MAPbI_3$ perovskite layer. The ETL-free devices also exhibited high photo stability in comparison to the conventional regular n-i-p architecture with TiO_2 based ETL.

2.8 Fabrication Methods

In the "one-step" deposition or spin coating method, the perovskite precursors of appropriate stoichiometry are prepared in a common solution and are then spin coated into a thin film (Figure 2.7a). Power conversion efficiency of over 20% has been achieved using this single step method. In the case of "two-step" deposition method or "sequential" deposition process, two precursor solutions are prepared. For instance, a thin film is first deposited using metal halide (e.g., PbI_2) precursor using spin coating process (mostly) and then the film coated substrate is dipped into the second precursor solution (Figure 7b). PSCs are also fabricated using the doctor blade method (PCE ~15%) and slot die coating (~12%), which could be a versatile approach for scalability. Dual source evaporation or vacuum deposition methods was also used to deposit perovskite thin films, which provided the advantage of producing pin-hole free layers with uniform thickness—resulting in PCE of ~15%. However, this method presents challenges for scalability and also requires relatively high energy for film fabrication. Hybrid approach of using both solution processing and vapor deposition to fabricate perovskite thin films was also developed. Here, the PbI_2 precursor is first spin-coated and then the methyl ammonium iodide (MAI) is evaporated on top of the as-deposited PbI_2 film and a PCE of ~12% was achieved using this method [38].

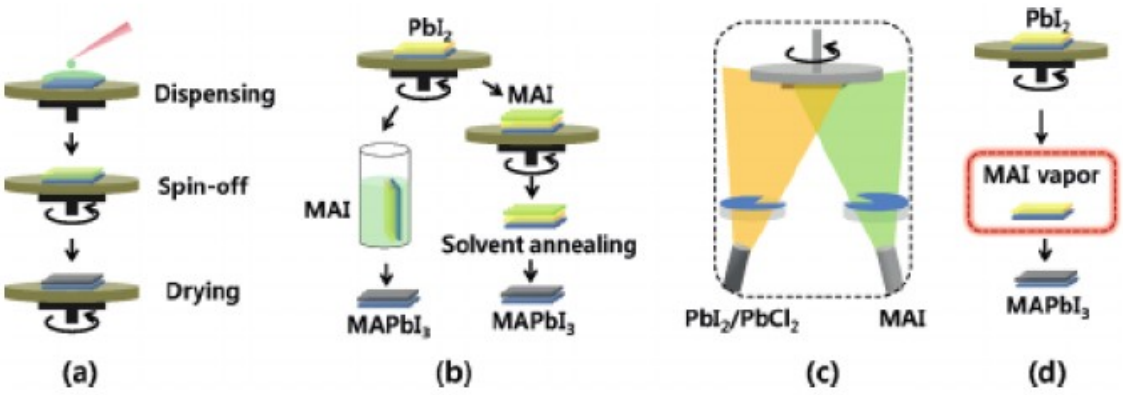

Figure 2.14 Representative fabrication methods for perovskite thin films: (a) one-step spin-coating method; (b) two step or sequential deposition method; (c) dual-source vapor deposition; and (d) vapor-assisted solution process [39].

CHAPTER 3

WxAMPS SIMULATION SOFTWARE

3.1 Simulation Software wxAmps

A comparatively new solar cell simulation program, wxAMPS, has been used for this work. The interface of wxAMPS uses a cross-platform library, wxWidgets, and the kernel is based on an updated version of the AMPS (Analysis of Microelectronic and Photonic Structures) code. wxAMPS incorporates two different tunneling models for better simulation of specific types of solar cells. Compared to the drift-diffusion model, the intra-band tunneling model provides more realistic characteristics for heterojunction solar cells. The other tunneling component is trap-assisted tunneling current, which plays an important role in tunneling recombination at junctions. To increase the convergence property of this model, a new algorithm that combines the Newton method and the Gummel method has been developed. The simulation results from different models are compared. A preliminary WIKI has also been set up, which provides a database of materials parameters for various kinds of solar cells to help the PV community share materials data and more easily implement simulations [40].

Some of the important features of wxAMPS is that the graphical user interface (GUI) of wxAMPS has been designed with a cross-platform C++ library, wxWidgets, and allows quick data entry as well as enhanced visualization of results for comparison and analysis. The main physical principles are derived from AMPS [41] and in addition two different tunneling models, intra-band tunneling [42] and trap-assisted tunneling [43], are incorporated to the program. The algorithm of wxAMPS has been modified to combine the Newton and Gummel methods, which improves convergence and stability. The effects of series and shunt resistance

unrelated to the main diode are also added. A database-oriented WIKI [44] has been set up for sharing the simulation files of devices and helping users find and discuss the parameters used in solar cell simulations. wxAMPS is a good tool to simulate various kinds and structures of solar cells, which can be made from crystalline and amorphous Si material, as well as CdTe and CIGS thin films, and other materials. Tandem structured solar cells can also be simulated through using the trap-assisted tunneling model in which carrier motilities are enhanced as functions of electric fields.

3.2 Interface

The main user interface (Figure 3.1) is almost the same as the version described in introduction with the exception of a "Settings" section under the Run button, allowing users to switch the tunneling models and adjust numerical parameters. In the "Settings" dialog box, users can set up upper limit of iteration times, the convergence precision and the clamping range that is the maximum variables change in one iteration. The variables variation is clamped in order to avoid the overestimation generated by the Newton method.

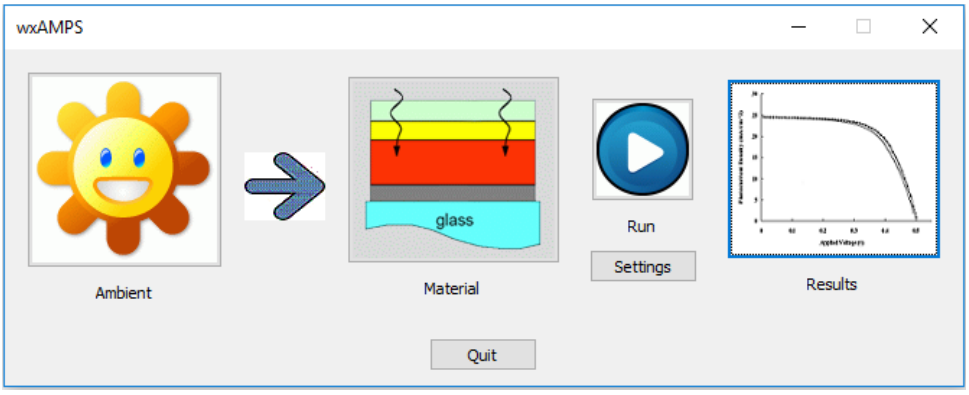

Figure 3.1 Main User Interface of wxAMPS

Another improvement is in the ambient dialog box where the bias voltages of interest can be loaded from a user customized text file. The ambient conditions configured previously by the user are cached automatically to help reduce the time spent tweaking the simulation environment. Among these settings, smaller voltage steps and clamping ranges can help improve the convergence property for a specific model, but at a cost of longer calculation time. Two additional slide bars have been added to the results dialog box in order to allow users to modify the values of the series and shunt resistances (Figure 2). Upon adjustment of the slide bars, a new current-voltage curve is calculated and displayed and new device parameters are obtained. The revised results and the new curve are updated simultaneously when changing the slide bars of the shunt and series resistances.

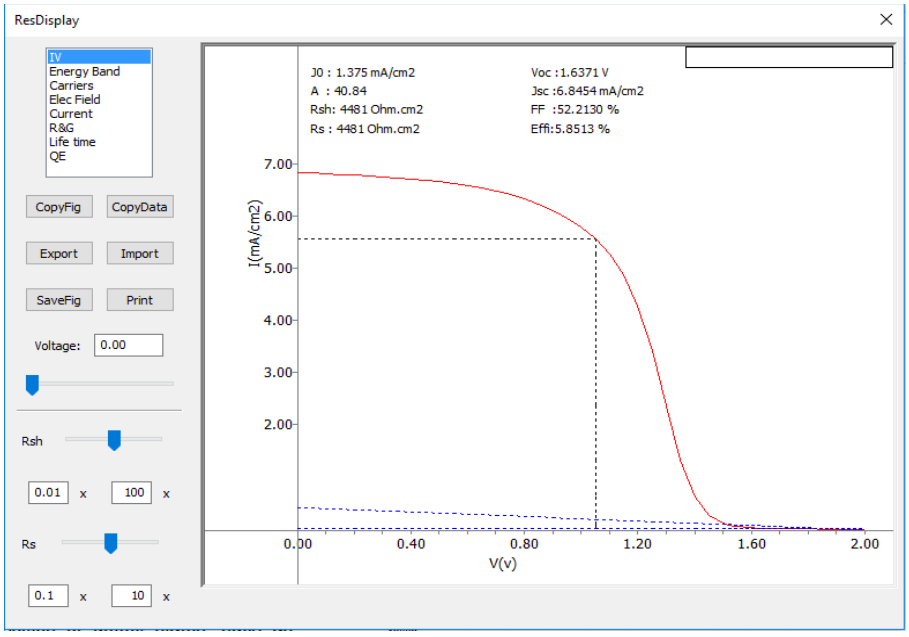

Figure 3.2 Display dialog box for simulation results and analysis

3.3 Selection of Input Parameters

3.3.1 Front and Back Contacts and Surfaces

In general, contacts can be assumed ohmic or, depending on the focus of the modeling, assigned a Schottky barrier height consistent with experimental observations. The reflection at the back surface has only minor influence on the achievable short-circuit current density (Jsc), and these influences only become noticeable if the absorber is chosen to be fairly thin. Many modeling tools support a constant multiplicative reflection factor for the front surface (i.e. RF = 0.1, 10% reflection). Quantum efficiency (QE) is then reduced by this fraction and, if interference effects are neglected, QE will show a fairly flat response at intermediate wavelengths of ~1-RF.

3.3.2 Material Parameters

Carrier mobilities for polycrystalline material should be chosen lower than the values reported for crystalline material. Effective masses of $m_e^* = 0.2m_0$ for electrons and $m_h^* = 0.8m_0$ for holes, which are numbers typical for direct band gap material, are recommended unless more specific data is available. The ratio of the carrier mobilities (μ_e/μ_h) should be approximately inversely proportional to the ratio of the effective masses (m_h^*/m_e^*). The effective density of states, NC, can be calculated using equation below [45] and similarly for NV. Note the direct temperature dependence in NC and NV, which should be taken into account for temperature dependent modeling.

$$N_C = 2\left(\frac{2\pi m_e^* kT}{h^2}\right)^{\frac{3}{2}} \tag{3.1}$$

Carrier concentrations can be determined from capacitance-voltage analysis. Typical numbers are in the authors' experience the order of 10^{16} cm^{-3} for CIGS and 10^{14} cm^{-3} for CdTe. The band gaps of the semiconductors are known, and for the $Cu(In_{1-x}Ga_x)Se_2$ alloys an approximate expression can be used. Band offsets at the interfaces will be discussed within the specific material sections below.

$$E(x) = 1.02 + 0.67x + 0.11x(x-1) \tag{3.2}$$

3.3.3 Defect States

Most numerical simulators use the Shockley-Read-Hall (SRH) model to describe carrier recombination currents. There are two approaches to do this: either the model assumes a constant minority carrier lifetime τ, or the input parameters are capture cross sections, σe and σp, and the defect distributions $N_{def}(E)$. An estimate of the lifetime (LT) can be calculated from the defect density (DD) parameters by

$$\tau \cong \left(\sigma v_{th} N_{def}\right)^{-1} \tag{3.3}$$

vth ≅ 10^7 cm/s is the thermal velocity of the electrons. However, in general the lifetime depends on the cross sections for both carriers and the Fermi level.

3.3.4 Defect Density (DD) Model

Since variations of the energetic defect distribution show only negligible effects on the output, it is recommended to position recombinative defect states in a narrow distribution close to the middle of the band gap (generic "mid-gap" states). In the SRH formalism, a defect state can change its charge state only by one elementary charge; therefore, one can always make the following distinctions: A donor-like (acceptor-like) defect state is likely to give away (accept) an additional electron. The two possible charge states for donors (acceptors) are positive and

neutral (negative and neutral). It follows that free electrons (holes) will be coulomb attracted to the ionized donor-like (acceptor-like) defect state, whereas holes (electrons) will have no strong interaction with the donor-like (acceptor-like) defects, giving very small hole (electron) crossections. The transition of a hole into the ionized donor-like defect, or the transition of an electron into a neutral donor-like defect is rare. One problem with the SRH picture is that physical impurities often generate several possible defect levels that have different charge states; however, a cross-linking between two or more energy levels is not contained in the SRH formalism.

$$\sigma_{att} = \frac{q^4}{16\pi\varepsilon_s^2 k^2 T^2} \approx 10^{-13} - 10^{-12}\ cm^2 \tag{3.4}$$

Neutral cross-sections can range between 10^{-18} and 10^{-15} cm2; the latter number corresponds to the physical size of an atom and is often referred to as “geometric” crossection. Smaller values account for quantum mechanical transition probabilities or compensate for strong field effects in the region of interest. In the Defect Density(DD) model, free carriers can be trapped in defect states, which alters the space charge distribution and leads to a deformation of the band structure. Illumination and/or voltage bias can alter the trapped carrier density, giving rise to transient effects. Mid-gap acceptor-like defect states in n-type material or mid-gap donor-like defect states in p-type material will completely ionize in thermal equilibrium unless the layer is strongly depleted or inverted. Often it is useful to compensate for the changes in free carriers and space charge by adjusting shallow donor (acceptor) densities.

3.3.5 The Lifetime (LT) model

It is in general easier to use since it requires only one input parameter. Lifetimes calculated by eqn. (3) do not always correspond to DD model simulations due to the approximation that went into the derivation of eqn. (3); in general lifetimes have to be chosen somewhat higher. Also, DD models usually calculate lifetimes that vary over several orders of magnitude within the same material, which violates the basic assumption of uniform lifetimes.

3.3.6 Surface recombination

Velocity at the front and back contact is chosen as V_{th}, which effectively recombines every minority carrier that reaches the contacts.

3.3.7 Tail states

Tail states are not incorporated in the baseline cases. They were found to be negligible contributors to the recombination current unless their density is several orders of magnitude larger than that of the mid-gap defect states [46].

3.4 Summary

With convenient user interface and the incorporation of the intra-band tunneling model and the trap-assisted tunneling model, wxAMPS is high performance software to simulate the behaviors of homo and heterojunction solar cells. The solar cell parameters predicted by these two tunneling models and traditional drift-diffusion model are very close if the device works in weak electrical fields as well as low currents, and without a high barrier at the hetero-interface.

CHAPTER 4

RESULTS AND ANALYSIS

4.1 Introduction

The organic-metal halide perovskite is emerging technology in photovoltaic solar cells. For any solar cell to get the significant efficiency depends on various design parameters such as material thickness, device architecture, doping concentration etc.. There are many solar cell simulation software which can be used to carry out simulation and thus optimization based on those parameters. Here for this research, we are using wxAMPS because it is freely available, simple, efficient and quite popular in solar cell research society. Keeping external parameters constant (one-sun, AM1.5G solar radiation, 1000 w/m^2 irradiation), numerical simulation and analysis of a perovskite solar cell with configuration Electron Transport Material (ETM)/Perovskite/Hole Transport Material (HTM) was carried out. In the proposed configuration Zinc oxide (ZnO) was used as Electron Transport Material (ETM), mixed halide perovskite ($CH_3NH_3PbI_{3-x}Cl_x$) was used as absorber material, and Copper thiocyanate (CuSCN) was used as Hole transport material (HTM). The performance of the solar cell was optimized using layer by layer optimization techniques. The results show a significant enhancement in conversion efficiency of 14.4% (Jsc = 15.44 mA/cm^2, Voc = 1.08 V, and FF = 0.85). The solar cell need further optimization which is under progress. However these simulation results can help researchers to reasonably choose materials and optimally design high-performance perovskite solar cells.

We have recently witnessed a breakthrough in highly efficient solar cells, where the organo-lead halide perovskite, $CH_3NH_3PbI_3$, was used as an absorber of sunlight. The perovskite was used to sensitize mesoporous TiO_2 films in a solid-state mesoscopic solar cell to deliver a power conversion efficiency (PCE) of up to 9.7%. A short period later, mesoporous Al_2O_3 was employed as a scaffold to support the formation of continuous thin films of a mixed halide perovskite, $CH_3NH_3PbI_{3-x}Cl_x$, to form non-sensitized solar cells. This so-called "meso-superstructure" perovskite solar cell had a PCE as high as 10.9%. This study showed that the mixed halide perovskite could function as both a light absorber and an electron absorber [46]. Most reported device architectures has adopted spiro-OMeTAD or PEDOT:PSS/ organic hole transporting layer, which is less than ideal owing to their tendency to absorb water, and inability to block electrons. Using P-type inorganic material such as copper thiocyanate (CuSCN) could be a long term solution for constructing stable perovskite-based solar cells [47]. Compared with organic spiro-OMETAD, inorganic p-type CuSCN with similar physical property, good chemical stability, ease of synthesis procedure and low cost is an ideal kind of hole transport material. Moreover CuSCN can be easily compatible with flexible substrates, which is deposited with a solution-processed technique at low temperature [48]. In this research I have proposed a new architecture of a perovskite solar cell using CuSCN as hole transport layer, mixed halide perovskite material $CH_3NH_3PbI_{3-x}Cl_x$ and ZnO as electron transport layer. In order to provide experimental guidance, we performed a theoretical study on band offset properties between perovskite materials and inorganic HTM by using wxAMPS (Analysis of Microelectronic and photonic structure). The wxAMPS program incorporates intra-band tunneling model and trap assisted tunneling model which provides more realistic characteristics for heterojunction solar cells.

4.2 Perovskite-Based Tandem Solar Cell

Tandem cells are solar cells made of multiple junctions with tunable absorbing materials, which aim to overcome the Shockley-Queisser single junction solar cells. Due to the respectful performance of perovskite-based solar cells, the design of perovskite/perovskite tandem solar cells emerges as a focal point in the research community, which is further fueled by the advancing perovskite manufacture technology. Every tandem solar cell have different sub cells. Here in this research two different perovskite solar cells are used. ZnO/$CH_3NH_3PbI_{3-x}Cl_x$/CuSCN solar cell was employed as a top cell with a recombination layer and PCBM/$MAPbBr_3$/$MAPbI_3$/CuSCN was employed as bottom cell. These two solar cells combined to form a tandem solar cell.

4.3 Top Cell of a Perovskite/Perovskite Tandem solar cell

Every solar cell has its own architecture which contains mainly Hole Transport Material(HTM), Electron Transport Material(ETM) and active layer or absorber layer. The solar cell with a perovskite layer sandwiched between ZnO and CuSCN is shown in figure.4.1. The perovskite layer is the absorber or active layer used in this solar cell [49]. The presence of HTM not only favors the hole transport but also blocks the electron transferring from the perovskite layer to the electrode, which can improve the PCE and V_{oc} of the devices. The instability of perovskite at high relative humidity is one issue that needs to be addressed. One method used to solve this problem is the creation of a mixed halide perovskite. The simple solution mixture of $CH_3NH_3PbI_3$ and $CH_3NH_3PbCl_3$ was reported to result in a solid solution of $CH_3NH_3PbI_{3-x}Cl_x$. Since triiodide and trichloride perovskite have a band gap difference, the

solid solution resulted in band gap tuning and color control. Also it was found to be a very unusual set of characteristics for the mixed halide perovskite $CH_3NH_3PbI_{3-x}Cl_x$ that indicate surprisingly clean semiconducting behavior and give excellent PV performance. This indicates that multiple electron-hole collisions can occur within the sample without nonradiative decay. This is a necessary criterion for photovoltaic operation close to the Shockley-Queisser limit, indicating significant future scope for these perovskite solar cells to reach the very highest solar power conversion efficiencies. In this solar cell Material used for Electron Transport layer (ETL) is Zinc Oxide (ZnO). It is a potential material for many applications due to their high electron mobility, transparent and various nanostructure. The ZnO was introduced into the perovskite solar cells structure to improve electron extraction efficiency. Material used for Hole Transport Layer (HTL) is copper thiocyanate (CuSCN). Copper Thiocyanate is an interesting material to be used as an inexpensive, thermally stable p-type charge conducting material in perovskite solar cells

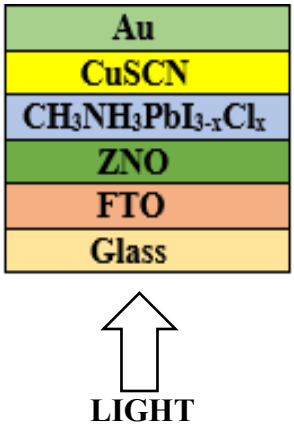

Fig.4.1 Perovskite solar cell architecture

4.4 Device Simulation Parameters

Many modeling tools support a constant multiplicative reflection factor for the front surface (i.e. RF = 0.1, 10% reflection). Quantum efficiency (QE) is then reduced by this fraction and, if interference effects are neglected, QE will show a fairly flat response at intermediate wavelengths of ~1-RF. The Architecture discussed in this paper is FTO/ZnO/$CH_3NH_3PbI_{3-x}Cl_x$/CuSCN/Au. Here FTO is fluorine doped tin oxide coated on glass as anti-reflective coating is used on top of the architecture. It also acts as cathode. Also we have used Electron Transport Material (ETM) as Zinc Oxide (ZnO) and Absorber as mixed halide perovskite ($CH_3NH_3PbI_{3-x}Cl_x$) and Hole Transport Material (HTM) as Copper thiocyanate (CuSCN). And at the bottom we have used gold (Au) metal as anode. The light reflection of the top and bottom contacts were set to be 0 and 1 respectively. The material parameters were summarized in table 4.1, most of which were selected from reported experimental works. The thickness of various layers were varied to find out their optimum values.

Table 4.1 Simulation Parameters of Top Cell Perovskite Solar Cells In This Study

Properties	**Symbol**	**CuSCN [48]**	**ZnO** [48]	**$CH_3NH_3PbI_{3-x}Cl_x$ [47]**
Dielectric Constant	ε_r	10	8.12	30
Band Gap	E_g (eV)	3.4	3.4	1.5
Electron Affinity	χ(eV)	1.9	4.29	3.93
Electron Mobility	$\mu_n(cm^2V^{-1}S^{-1})$	0.0001	2-30	14
Hole Mobility	$\mu_h(cm^2V^{-1}S^{-1})$	0.1	2	14
Acceptor Concentration	$N_A(cm^{-3})$	5×10^{18}	9×10^{16}	6×10^{14}
Donor Concentration	$N_D(cm^{-3})$	0	10^{19}	0
Effective Conductive Band Density	$N_c(cm^{-3})$	1.7×10^{19}	3.7×10^{18}	2.5×10^{20}
Effective Valence Band Density	$N_v(cm^{-3})$	2.5×10^{21}	3.7×10^{18}	2.5×10^{20}

4.5 Results

The results are obtained by method of optimization technique. The thickness of the perovskite is varied from 350nm to 750nm. The perovskite thickness optimization curves are shown in fig.4.2.

A) Optimization of perovskite thickness

Thickness of a material plays a major role in performance of solar cells. The active layer i.e. perovskite layer thickness is varied from 350 nm to 750 nm. As the thickness increases the performance of the solar cell increases which has been shown in fig.4.2. At a certain thickness of 600 nm solar cell performance began to decrease.

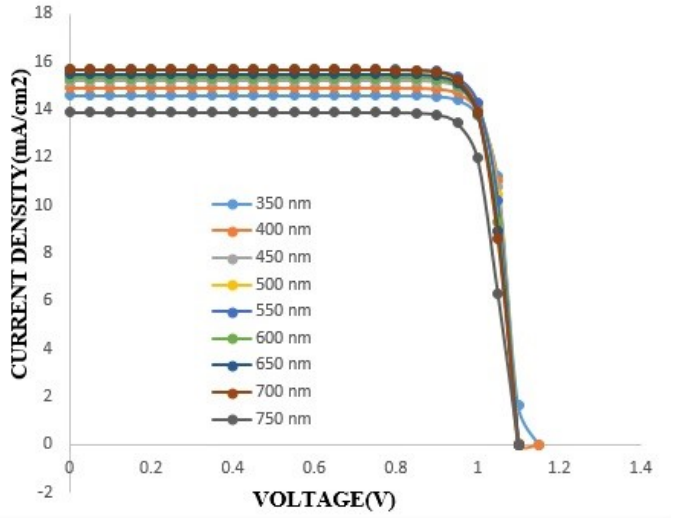

Fig.4.2 Perovskite thickness optimization curves

Therefore the optimum thickness of this perovskite solar cell is 550 nm. The simulated Jsc and PCE of $CH_3NH_3PbI_{3-x}Cl_x$ with varying perovskite thickness are shown in fig.4.3 The first graph is obtained by giving thickness values on x-axis and current density on y-axis. When the thickness was increasing, the current density was also increasing and the maximum current density was obtained when thickness of mixed halide layer was close to 550 nm as function of

thickness of layer . The second graph is obtained by giving thickness values on x-axis and power conversion efficiency on y-axis. When the thickness was increasing power conversion efficiency also increasing and maximum power conversion efficiency was obtained when thickness of mixed halide layer was close to 550 nm. The power conversion efficiency is 14.4% at 550nm. The third graph is obtained by varying thicknesses with open circuit voltage. When the thickness was increasing the open circuit voltage was decreasing. Open circuit voltage was measured at the optimum thickness of mixed halide perovskite layer i.e 550 nm.

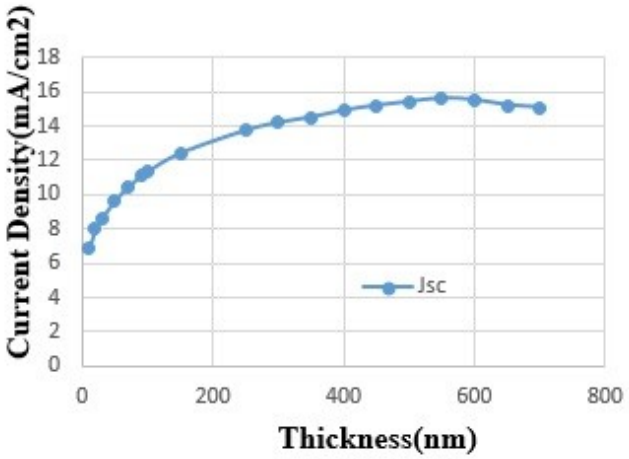

Fig.4.3 The current density of perovskite solar cell as function of thickness of mixed halide $CH_3NH_3PbI_{3-x}Cl_x$ layer.

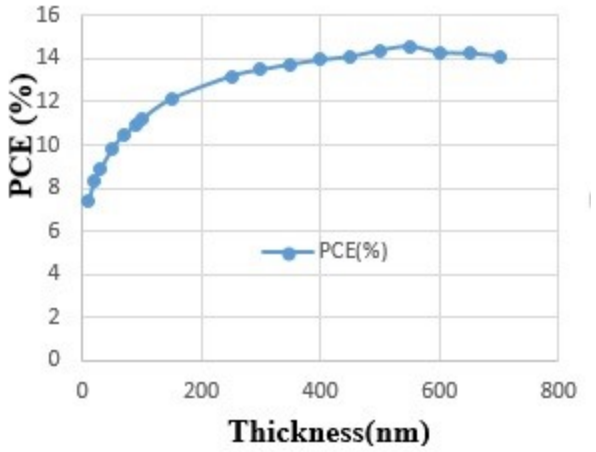

Fig.4.4 The power conversion efficiency of perovskite solar cell as function of thickness of mixed halide $CH_3NH_3PbI_{3-x}Cl_x$ layer.

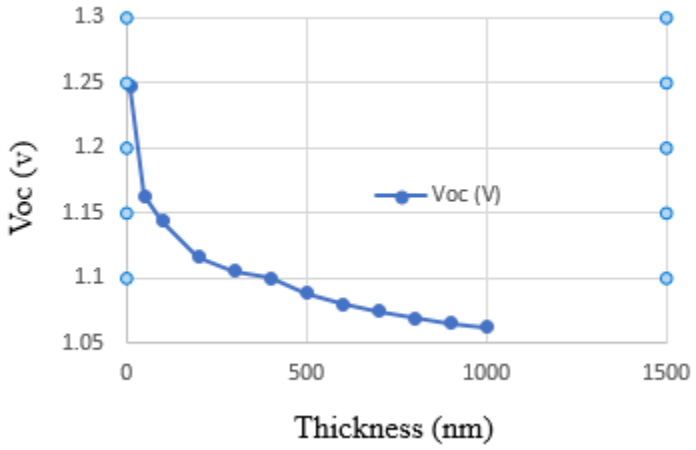

Fig. 4.5 The open circuit voltage of perovskite solar cell as a function of thickness of $CH_3NH_3PbI_{3-x}Cl_x$ layer.

B) Energy Band curves of a perovskite solar cell

The energy band curves are obtained by presenting energy (eV) values on y-axis and position X(um) values on x-axis. The energy band diagram of the perovskite solar cell at

thermal equilibrium is shown in figure.4.5. This figure shows the positions of conduction band, valance band and fermi level. The energy band diagram vary significantly than the typical PN junction solar cell, indicating that band analysis for perovskite solar cell need to be carried out in a different way, which has been suggested as a future work.

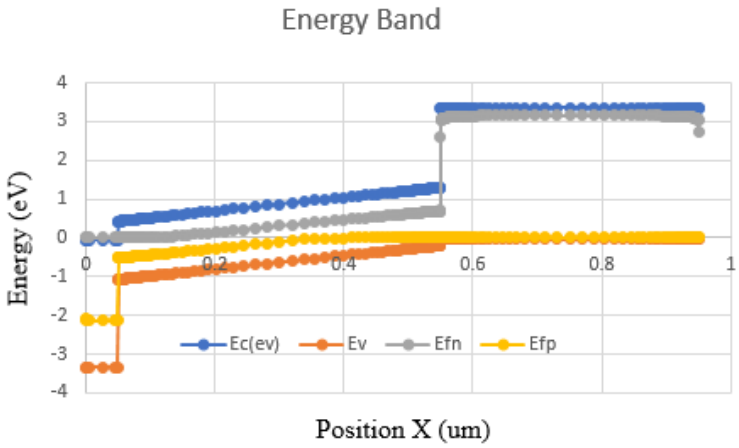

Fig.4.6 Energy (eV) of perovskite solar cell as a function of position (um) or distance in the perovskite solar cell.

C) Electric Field curves of a perovskite solar cell

The electric field curves are obtained by presenting electric field (V/cm) values on y-axis and position X (μm) on x-axis. The built in electric field distribution curve of this perovskite solar cell is shown in figure.4.6. By analyzing the curve it is found that the electric field is high when absorption layer thickness is about 0.55μm. So the optimized thickness value of absorption layer results in high efficiency.

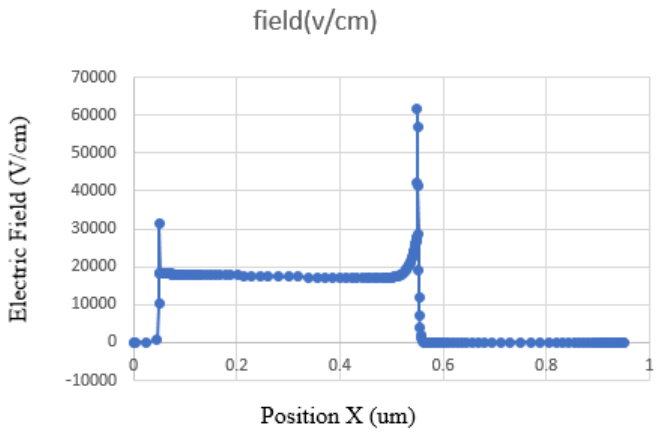

Fig.4.7 Electric Field curves of a perovskite solar cell

D) Current Density curves of a perovskite solar cell

The current density of a simulated perovskite solar cell is 15.48 mA/cm^2. Figure 4.7 shows that current density of electron and current density of hole and total current density. The result of these two curves give the total current density of a perovskite solar cell. Electron current density is high in the n-type region and gradually decreases in p-type region. Hole current density is low in n-type region and significant increase in p-type region. The result of this two curves give the total current density of perovskite solar cell.

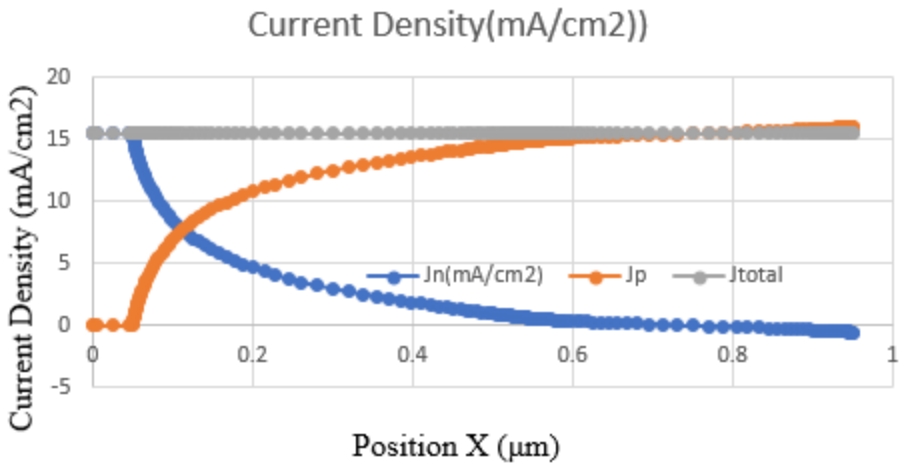

Fig. 4.8 Current density of perovskite solar cell as a function of position or depth of the perovskite solar cell.

E) Quantum Efficiency of the perovskite solar cell

Quantum efficiency of a solar cell indicates the amount of current that the cell produce when irradiated by photons of a particular wavelength. The figure shows that the conversion ratio of photons to electrons, i.e. QE within the wavelength range of 250 to 1000 nm. Below 250 and above 1000 nm, light absorption is negligible for this type of solar cell. The figure shows that the solar cell photon absorption capacity of 250 to ~900 nm. QE is found to be high and steady (above 90%) between the wavelengths 250 to 575 nm. After that the quantum efficiency gradually decreases sharply up to 750 nm. In this case, the quantum efficiency drop from 90 % to below 10%. The overall QE of this solar cell indicate that it can absorb photon and effectively convert into electron in both UV and visible region, which is a very important quality of high performance solar cell.

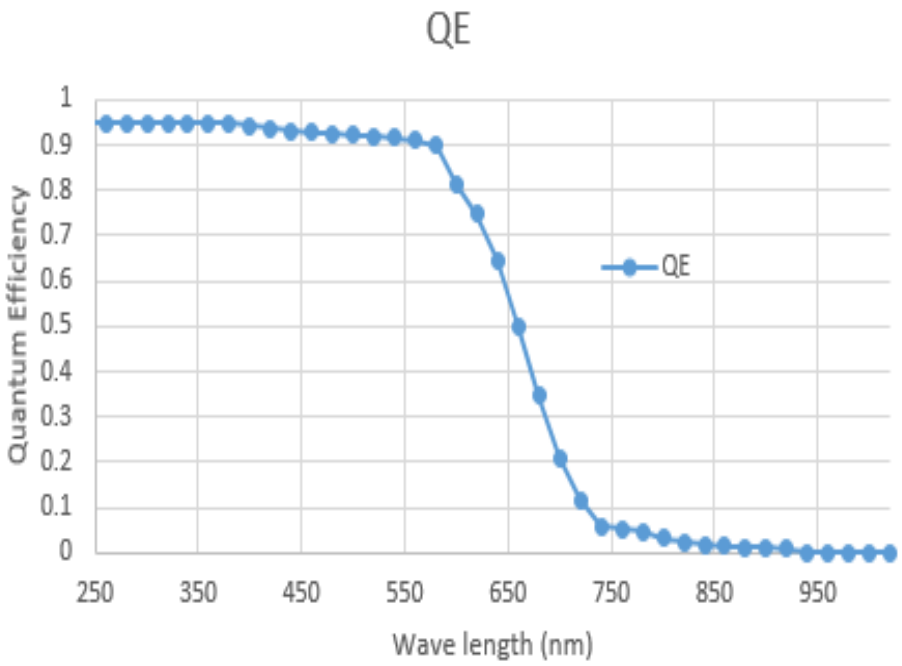

Fig.4.9 This graph shows the variation of quantum efficiency with wavelength of a perovskite solar cell.

F) Solar cell Performance on defects in perovskite materials

The density and property of defects in perovskite material play a crucial role due to photoelectrons being mainly generated and recombined in light absorber. The Gaussian distribution is more suitable to describe these defect states because of exiting a lot of defect energy levels in the perovskite. So we assumed that there are both acceptor states and donor states modeled by Gaussian mid-gap states. The simulation results for J-V characteristics with various defect density are shown in fig.4.8. It shows that PCE , Jsc, Voc attain maximum values when the defect density is 10^{14} cm^{-3}. The increasing of defect density brings about the drop of PCE, Jsc, Voc of perovskite solar cell. The ideal defect density value for perovskite is $10^{14}cm^{-3}$. The materials having less defect density are the best materials to use in a solar cell. Here perovskite material have very less defect density when compared to other materials. Hence this is one of the reasons to select perovskite material.

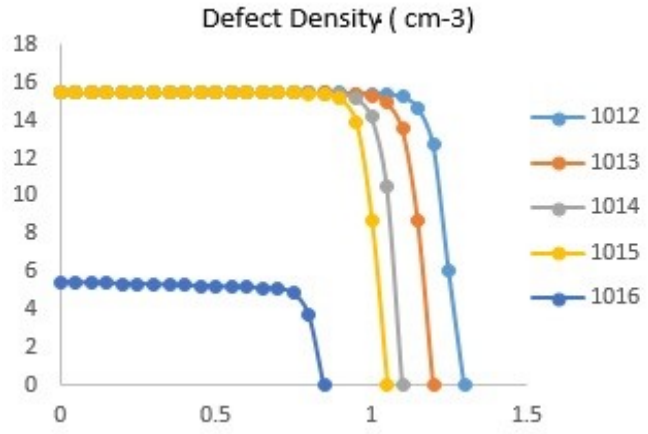

Fig.4.10 The J-V characteristic curves for solar cells as a function of defect densities in perovskite materials.

By giving the inputs like electrical, optical parameters of each layer such as ETM, Absorber, HTM we have obtained a conversion efficiency of 14.4% (JSC = 15.44 mA/cm 2, VOC = 1.08 V, and FF = 0.85). The Dark and Illuminated I-V Characteristics of this perovskite solar cell is determined in the graph below.

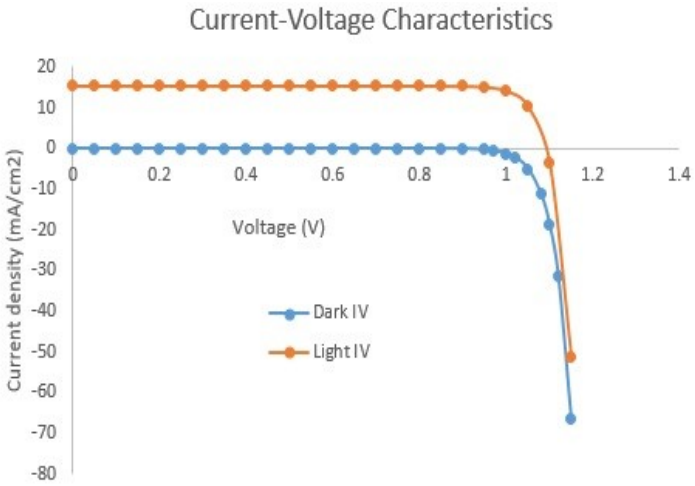

Fig.4.11 The J-V characteristics curves for perovskite solar cell.

4.6 Bottom cell of a Perovskite/Perovskite Tandem solar cell

The bottom cell of perovskite-based solar cell contains PCBM (fullerene derivative [6,6]-phenyl-C_{61}-butyric acid methyl ester) is used as an Electron Transport Layer (ETL). And the perovskite layers $MAPbBr_3$ or $CH_3NH_3PbBr_3$ (Methyl Ammonium Lead Bromide) and $MAPbI_3$ or $CH_3NH_3PbI_3$ (Methyl Ammonium Lead Iodide) are used as absorbent layers. And Copper thiocyanate (CuSCN) is used as a Hole Transport Layer (HTL). These stack of layers are shown in figure below.

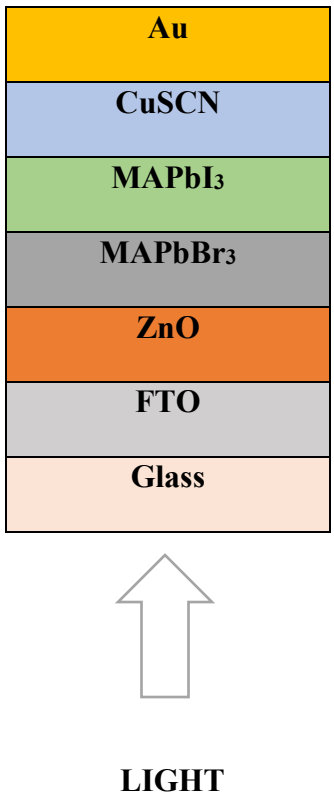

Fig. 4.12 Bottom cell perovskite solar cell architecture

Many modeling tools support a constant multiplicative reflection factor for the front surface (i.e. RF=0.1, 10% reflection). Quantum efficiency (QE) is then reduced by this fraction and, if interference effects are neglected, QE will show a fairly flat response at intermediate wavelengths of ~1-RF. The Architecture discussed was FTO/PCBM/$MAPbBr_3$/$MaPbI_3$/CuSCN/Au. Here FTO is fluorine doped tin oxide coated on glass as anti-reflective coating is used on top of the architecture . It also acts cathode. The light reflection of the top and bottom contacts were set to be 0 and 1 respectively. The material parameters were summarized in table below., most of which were selected from reported experimental works. The thickness of various layers were varied to find out their optimum values.

Table 4.2 Simulation Parameters of Bottom cell Perovskite solar cell

Properties	**Symbol**	**CuSCN [48]**	**ZnO[47]**	**$MAPbBr_3$[48]**	**$MAPbI_3$[48]**
Dielectric Constant	ε_r	10	9	23.3	28.7
Band Gap	E_g (eV)	3.4	3.3	1.51	2.22
Electron Affinity	χ(eV)	1.9	4.4	3.93	3.36
Electron Mobility	μ_n($cm^2V^{-1}S^{-1}$)	0.0001	10	50	19
Hole Mobility	μ_h($cm^2V^{-1}S^{-1}$)	0.1	2.5	50	19
Acceptor Concentration	N_A(cm^{-3})	5×10^{18}	0	2.14×10^{17}	2.14×10^{17}

Donor Concentration	$N_D(cm^{-3})$	0	1×10^{18}	0	0
Effective Conductive Band Density	$N_c(cm^{-3})$	1.7×10^{19}	2.2×10^{18}	1.66×10^{19}	2.18
Effective Valence Band Density	$N_v(cm^{-3})$	2.5×10^{21}	1.8×10^{19}	5.4×10^{18}	7.82×10^{18}

A) The Energy Band curves of a bottom cell perovskite solar cell

The energy band curves are obtained by presenting (eV) values on y-axis and position X (um) values on x-axis. The energy band diagram of the perovskite solar cell at thermal equilibrium is shown in figure below. This figure shows the positions of conduction band, valance band and fermi level. The energy band diagram vary significantly than the typical PN junction solar cell, indicating that band analysis for perovskite solar cell, indicating that band analysis for perovskite solar cell need to be carried out in a different way, which has been suggested as a future work.

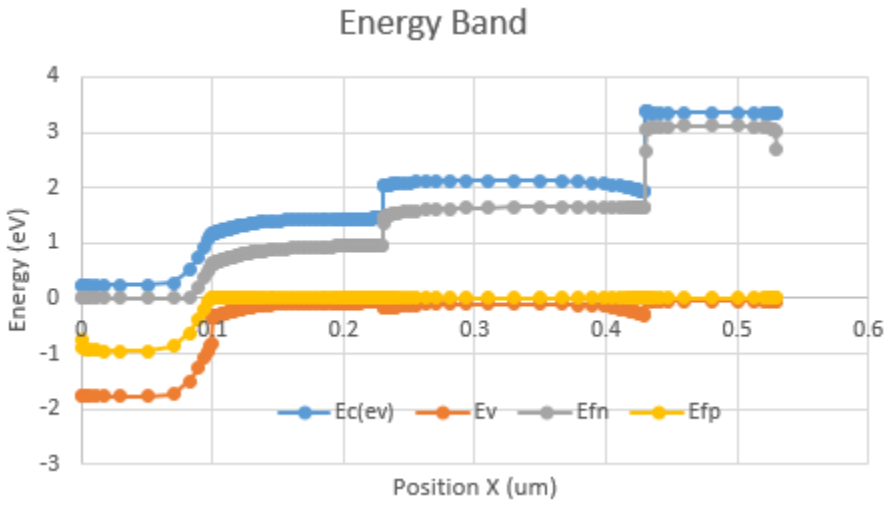

Fig.4.13 Energy (eV) of perovskite solar cell as function of position X (um) or depth of the perovskite solar cell.

B) Electric Field curves of Bottom cell perovskite solar cell

The electric field curves are obtained by presenting electric field (V/cm) values on y-axis and position X(um) on x-axis. The built in electric field distribution curve of this perovskite solar cell is shown in figure below. The conclusions drawn after analysis of the curves found that the electric field is high when absorption layer thickness is from 130 nm to 200 nm. So the optimized thickness value of absorption layer results in high efficiency.

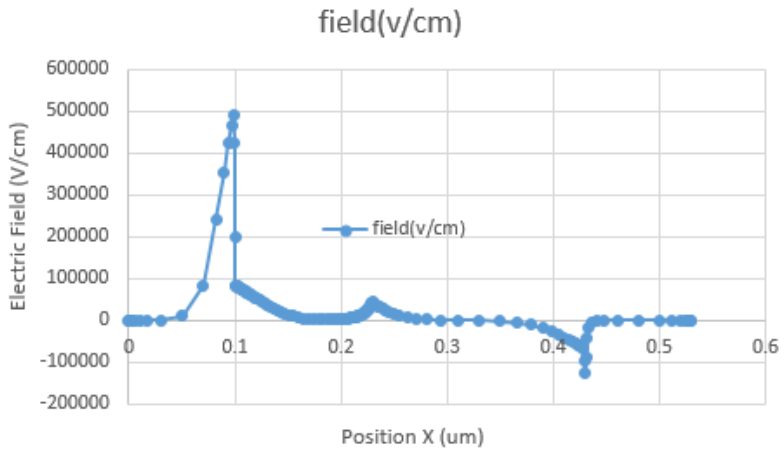

Fig. 4.14 Electric Field of perovskite solar cell as a function of position or depth of the perovskite solar cell.

C) Current Density curves of bottom cell perovskite solar cell

The current density of a simulated perovskite solar cell is 13.19 mA/cm^2. Fig. 4.13 shows that current density of electron and current density of hole and total current density. Current density of electron is high in the electron transport layer and current density of hole is

high in hole transport layer. The result of these two curves give the total current density of a perovskite solar cell. Electron current density is high in the n-type region and gradually decreases when comes to p-type region. Hole current density is low in n-type region and significant increase in p-type region. The result of this two curves give the total current density of perovskite solar cell.

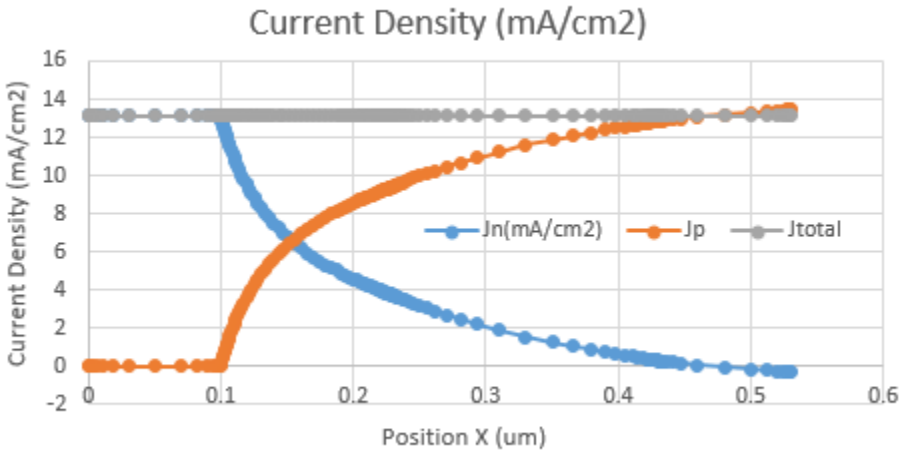

Fig. 4.15 Current density of perovskite solar cell as a function of position or depth of the perovskite solar cell.

D) Quantum Efficiency of the perovskite solar cell

The figure shows that the conversion ratio of photons to electrons, i.e. QE within the wavelength range of 250 to 1000 nm. Below 250 and above 1000 nm, light absorption is negligible for this type of solar cell. The figure shows that the solar cell photon absorption capacity of 250 to ~800 nm. QE is found to be high and steady (above 90%) between the wavelengths 250 to 625 nm. After that the quantum efficiency gradually decreases sharply up to 750 nm. In this case, the quantum efficiency drop from 90 % to below 20%. The overall QE

of this solar cell indicate that it can absorb photon and effectively convert into electron in both UV and visible region, which is a very important quality of high performance solar cell.

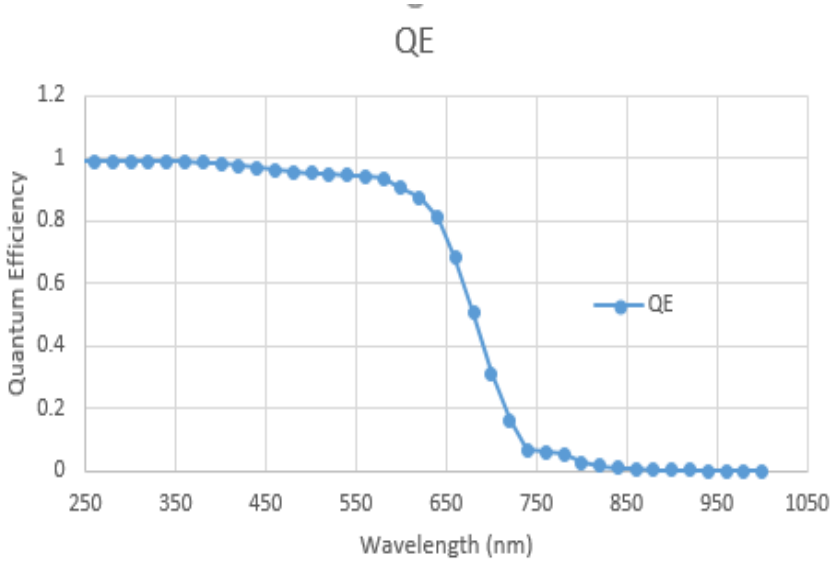

Fig.4.16 This graph represents the variation of quantum efficiency with wavelength of a perovskite solar cell.

E) J-V Characteristics of bottom cell perovskite cell

By providing with the inputs like electrical, optical parameters of each layer such as Electron Transport Layer, Absorber layer and Hole Transport Layer., we have obtained a conversion efficiency of 13.7% (J_{sc}= 13.19mA/cm^2, V_{oc}= 1.16V, and FF= 0.89). The dark and illuminated J-V characteristics of this perovskite solar cell is determined in the figure below.

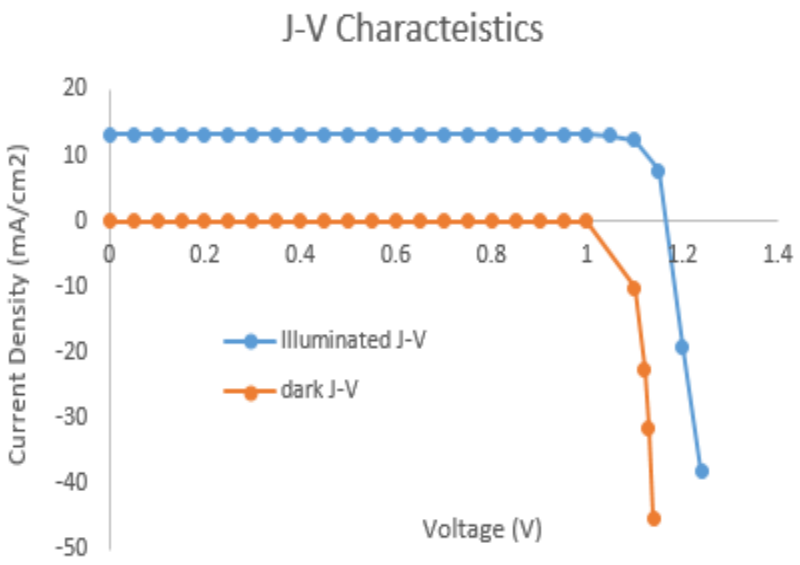

Fig. 4.17 The J-V Characteristics dark and illuminated curves of bottom cell perovskite solar cell.

4.7 Perovskite/Perovskite Tandem solar cell

The architecture of the perovskite/perovskite tandem solar cell is shown in figure below. The top cell is ZnO/$CH_3NH_3PbI_{3-x}Cl_x$/CuSCN and the bottom cell is ZnO/$MAPbBr_3$/$MAPbBr_3$/CuSCN. This figure shows the architecture of a perovskite based tandem solar cell. ZnO layer in the bottom cell was removed because the recombination layer acts as an electron transport layer. Recombination layer is typically made of combination of electron and hole transport layer and act as tunnel junction, (or bridge) connecting two consecutive solar cell. It helps increase electron and hole mobility thus facilitating their efficient recombination.

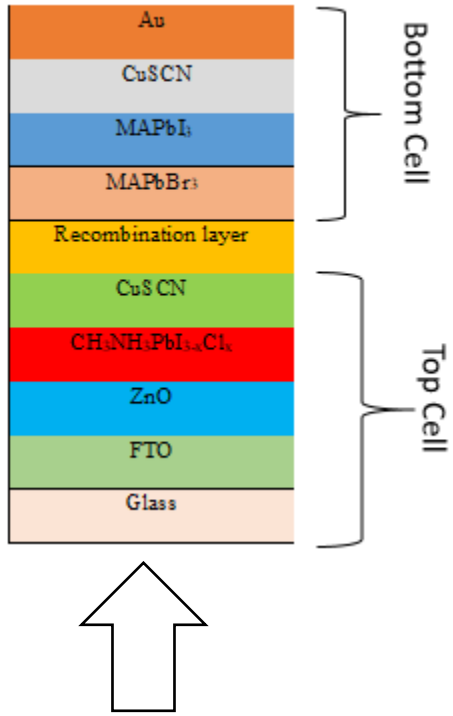

Fig.4.18 Perovskite based Tandem solar cell architecture

A) J-V Characteristics perovskite based tandem solar cells

The figure shows that the conversion ratio of photons to electrons, i.e. QE within the wavelength range of 250 to 1000 nm. Below 250 and above 1000 nm, light absorption is negligible for this type of solar cell. The figure shows that the solar cell photon absorption capacity of 250 to ~950 nm. QE is found to be un usually high (above 100%) between the wavelengths 250 to 450 nm. From 250 nm to 350 nm the QE is high and steady at ~110%. From 350 nm to 450 nm the QE is still above 100 %, i.e. drop from 110% to 100%, and this is a steady decrease. This phenomena might be attributed to the multi exciton generation by a high energy single photon in certain PV material and cell structure. Typically when a photon with energy more than twice of the band gap absorbed by a semiconductor and result in generation

of two electron-hole pair. So in this case, the generated current is twice the photon absorbed. In this case photon with wave length 250 to 450 are high energy UV photons. After that the quantum efficiency gradually decreases e.g. from 475nm to 725 the QE is above 90% then it start decreasing sharply up to 850 nm. In this case, the quantum efficiency drop from 90 % to below 20%. The overall QE of this solar cell indicates that the tandem structure is very efficient, particularly in UV region, to absorb photon and effectively convert into multi exciton. In visible region tandem structure shows significantly high QE, which is a very important quality of high performance solar cell

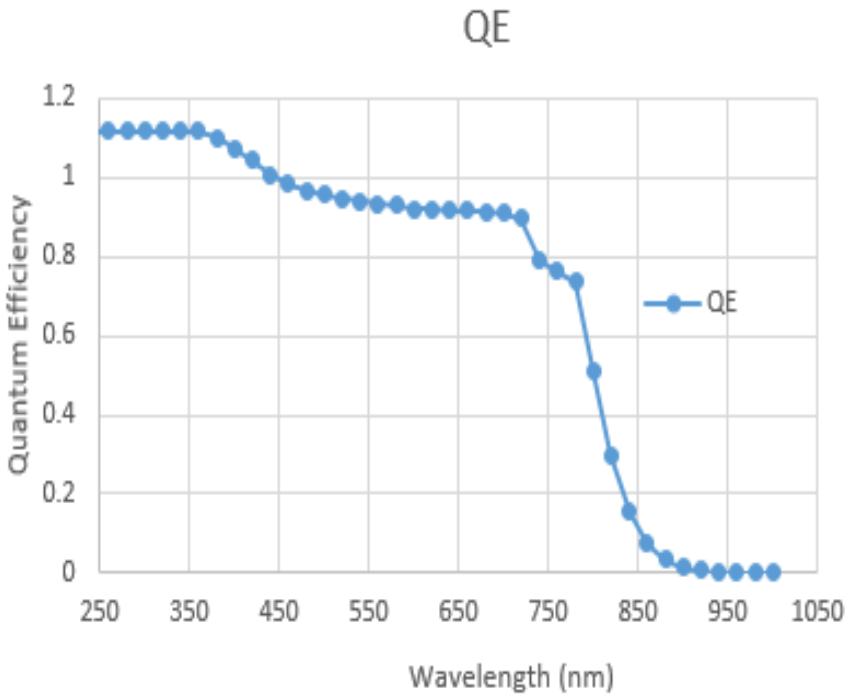

Fig.4.19 The variation of quantum efficiency with wavelength of a perovskite solar cell.

4.8 4 -Terminal Perovskite/Perovskite Solar cell

The 4- terminal stacked perovskite solar cells is shown in Figure 4.18. In this type of 4-terminals stack solar cell two similar perovskite solar cells are stacked (often mechanically) together on to one another with help of an intermediate layer. This intermediate layer is not a recombination layer/tunnel junction, it is transparent non conductive layer just separating two cells. The advantage of this type of solar cell is that the terminals can be connected in series or in parallel as required. Series connection will help double the voltage while current remains same. Parallel connection will help double the current while voltage remains same In both cases the efficiency will be double compared to the individual single solar cell. In a typical Perovskite Multijunction Solar Cell, for sub cells connected in series

- Short circuit current density Jsc-multi=Min[Jsc1,Jsc2,Jsc3……]
- Open circuit voltage, Voc-multi =Voc1+ Voc2+ Voc3+…….

for sub cells connected in parallel

- Short circuit current density Jsc-multi=[Jsc1+Jsc2+Jsc3+……]
- Open circuit voltage, Voc-multi =Min[Voc1+ Voc2+ Voc3+…….

where Jsc1, Jsc2, Jsc3….and Voc1, Voc2, Voc3….are short circuit current densities and open circuit voltages of sub cell 1, 2, 3… etc.

Efficiency of a PMSC is expressed as:

$$\eta_{multi} = \frac{J_{sc-multi} \cdot V_{oc-multi} \cdot FF}{P_{light}}$$

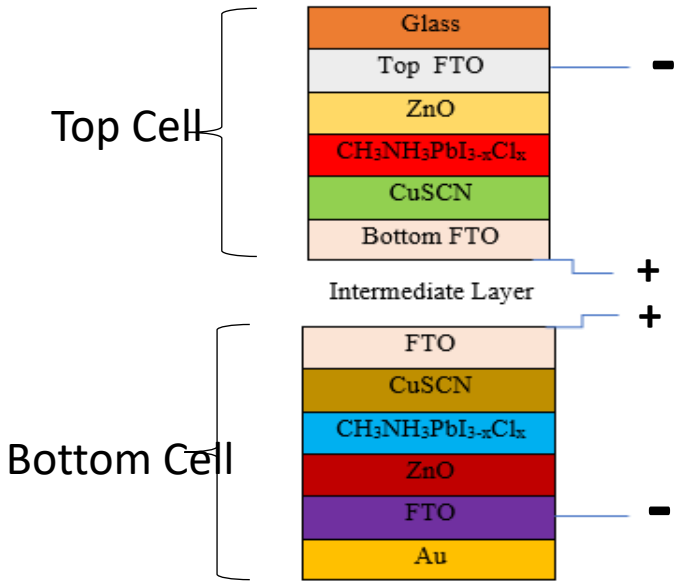

Fig. 4.20 The architecture of a 4 – terminal Perovskite/Perovskite solar cell

4.9 J-V Characteristics of a series connected stacked solar cell

This J-V is the result of stacking the top solar cell of the tandem structure previously described. From that J-V curve Maximum voltage current values are drawn. Also open circuit Voltage and short circuit current values are drawn from the J-V curve. From the values of Voc, Isc, Vmp, Imp we need to find out Fill Factor. Fill Factor = Vmp*Imp/Voc*Isc = 2*14.29/2.2*15.44 = 83.6% or 0.83. FF = (Vmp*Imp/Voc*Isc) = 2*14.29/2.2*15.44 = 83.6% or 0.83 Efficiency = Voc*Isc*FF/Pinput = 2.2*15.44*0.83/100 =28.19%. Hence theoretically for a selected perovskite stack solar cell the efficiency is 28.19% which is almost double compared to its single junction counterpart (14.4%)

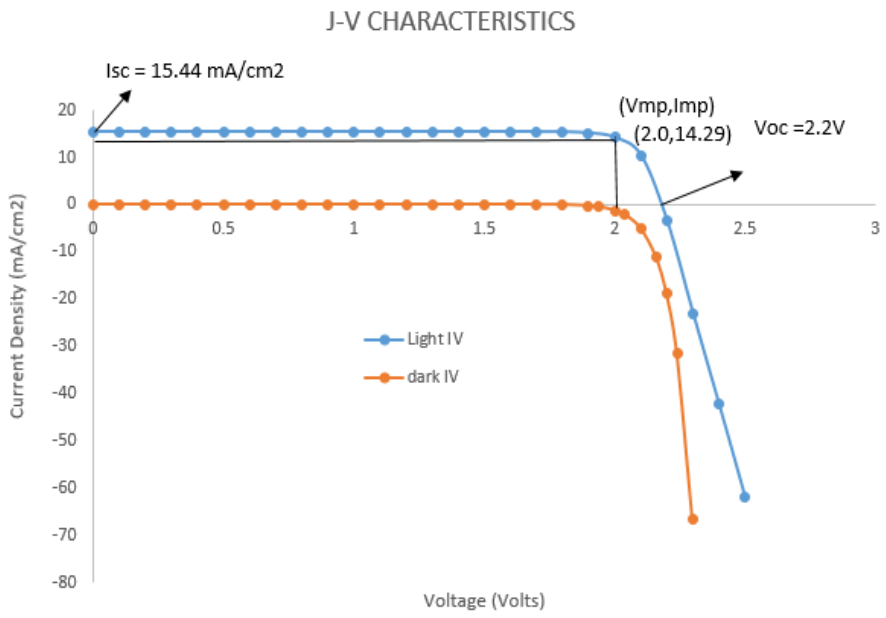

Fig.4.21 The J-V characteristics of 4-Terminal Perovskite/Perovskite stack solar cell

CHAPTER 5

CONCLUSION AND FUTURE WORK

5.1 Conclusion

Numerical Simulation and optimization of perovskite solar cell was performed using layer by layer optimization and results were obtained. For a perovskite solar cell the material used for absorber layer is mixed halide perovskite ($CH_3NH_3PbI_{3-x}Cl_x$). We find a very unusual set of characteristics for the mixed halide perovskite $CH_3NH_3PbI_{3-x}Cl_x$ that indicate surprisingly clean semiconducting behavior and give excellent PV performance. This indicates that multiple electron-hole collisions can occur within the sample without nonradiative decay. This is a necessary criterion for photovoltaic operation close to the Shockley-Queisser limit, indicating significant future scope for these perovskite solar cells to reach the very highest solar power conversion efficiencies. And Material used for Electron Transport layer (ETL) is Zinc Oxide (ZnO). It is a potential material for many applications due to their high electron mobility, transparent and various nanostructure. The ZnO was introduced into the perovskite solar cells structure to improve electron extraction efficiency. And material used for Hole Transport Layer (HTL) is copper thiocyanate (CuSCN). Copper Thiocyanate is an interesting material to be used as an inexpensive, thermally stable p-type charge conducting material in perovskite solar cells. Obtained results shows that copper thiocyanate could be a suitable choice for perovskite solar cells. An efficiency of 14.4% could be achieved, which shows potential of using CuSCN as an alternate hole transport material. This study also provides important theoretical guidance for new mixed halide perovskite has an good absorption properties and researchers can optimize for good results.

Single junction solar cell with architecture ZnO/$CH_3NH_3PbI_{3-x}Cl_x$/CuSCN was successfully simulated by using wxAMPS. Helped to optimize the thickness of a perovskite material. And obtained an efficiency of 14.4%(Jsc=15.44mA/cm2, Voc=1.08Volts, FF= 0.85) used as top cell of tandem structure. Another Single junction Solar cell with ZnO/$MAPbI_3$/$MAPbBr_3$/CuSCN was successfully simulated by using wxAMPS. Significant increase in the efficiency of 13.5% (Voc= 1.17V, Jsc= 13.19 mA/cm2, FF= 0.88). Perovskite-Based tandem solar cell was simulated by combining the above two solar cells gives best results. with an efficiency of 19.1% (Voc=0.95Volts, Jsc=24.14mA/cm2, FF= 0.83%). perovskite based tandem structure helped to increase efficiency significantly, for the first time we got such results With above mentioned individual solar cells. Using a freely available tool like wxAMPS

5.2 Future Work

Further studies on perovskite solar cells is introduction of organic-inorganic perovskite-based tandem solar cells. Tandem cells are the solar cells made of multiple junctions with tunable absorbing materials, which aim to overcome the Shockley-Quiesser limit of single junction solar cells. Organic-inorganic hybrid perovskite solar cells have stirred enormous interest as ideal for tandem cells due to high open circuit voltage, relatively wide optical bandgap, and low temperature solution processibility. These single junction devices can be used to make multijunction and should be simulated to predict the devices performance. Hence double Tvriple or quadruple junction solar cell should be need to be simulated. Recombination layer and active layer thickness should be optimized matching short circuit current and absorption properties. Proposed concept can be used to fabricate real solar to validate the simulation results. Employing a narrower bandgap perovskite and adopting a multijunction

approach would be likely to push the Power Conversion Efficiency (PCE) of perovskite solar cells.

Find a ways to employ different parameters like DOS, defects, absorption coefficient of perovskite materials in wxAMPS. Develop add in (Excel or MATLAB based simple and small software) for this type of solar cell to use with this software. Carry out experimental study to compare the result and adjust different parameters in simulation. Carry out more simulation and optimization with emerging and more environmental friendly perovskite materials based solar cell. Carry out simulation with triple or quadruple junction solar cell.

REFERENCES

[1] M. K. Siddiki, Ph.D Thesis "All Solution Processible Polymer Multijunction Solar Cells," South Dakota State University, 2012.

[2] M. H. Ibliha, M.S Thesis "Solar Cells With Novel Buffer Layers," University of Missouri-Kansas City, 2015.

[3] M. De Bastiani, Ph . D . Thesis "The Stability of Third Generation Solar Cells Università degli Studi di Padova," October, 2016.

[4] C. Spiegel, "Horizon Energy Curriculum." [Online]. Available: https://www. horizoncurriculum.com/chapter-2/2-1-introduction/.

[5] H. Zhu, J. Wei, K. Wang, and D. Wu, "Applications of Carbon Materials in Photovoltaic Solar cells," *Sol. Energy Mater. Sol. Cells*, vol. 93, no. 9, pp. 1461–1470, Sep. 2009.

[6] Y. Ma *et al.*, "Recent Research Developments of Perovskite Solar Cells," *Chinese J. Chem.*, vol. 32, no. 10, pp. 957–963, 2014.

[7] S. Razza, S. Castro-Hermosa, A. Di Carlo, and T. M. Brown, "Research Update: Large-Area Deposition, Coating, Printing, and Processing Techniques for the Upscaling of Perovskite Solar Cell Technology," *APL Mater.*, vol. 4, no. 9, 2016.

[8] G. Grancini *et al.*, "One-Year Stable Perovskite Solar Cells by 2D/3D Interface Engineering," *Nat. Commun.*, vol. 8, p. 15684, Jun. 2017.

[9] S. Rühle, "Tabulated Values of the Shockley–Queisser Limit for Single Junction Solar Cells," *Sol. Energy*, vol. 130, pp. 139–147, Jun. 2016.

[10] M. Kianinia *et al.*, "Robust Solid-State Quantum System Operating at 800 K," *ACS*

Photonics, vol. 4, no. 4, pp. 768–773, Apr. 2017.

[11] S. Li and J. Hu, "Immobilization of Hemoglobin on Cobalt Nanoparticles-Modified Indium Tin Oxide Electrode: Direct Electrochemistry and Electrocatalytic Activity," *Chem. Res. Chinese Univ.*, vol. 29, no. 3, pp. 563–567, Jun. 2013.

[12] Y. Nicolas *et al.*, "New Synthetic Routes Towards Soluble and Dissymmetric Triphenodioxazine Dyes Designed for Dye-Sensitized Solar Cells," *Chem. - A Eur. J.*, vol. 20, no. 13, pp. 3678–3688, Mar. 2014.

[13] X. Zhang *et al.*, "Molecular Engineering of New Phenothiazine-Based D–A–π–A Dyes for Dye-Sensitized Solar Cells," *RSC Adv.*, vol. 6, no. 108, pp. 106380–106386, 2016.

[14] K. W. Böer, "Solar Cells," *Chemistry - A European Journal*. .

[15] M. Sessolo and H. J. Bolink, "Perovskite Solar Cells Join The Major League," *Science* vol. 350, no. 6263, pp. 917–917, Nov. 2015.

[16] S. J. Yoon, K. G. Stamplecoskie, and P. V. Kamat, "How Lead Halide Complex Chemistry Dictates the Composition of Mixed Halide Perovskites," *J. Phys. Chem. Lett.*, vol. 7, no. 7, pp. 1368–1373, Apr. 2016.

[17] X. Zhu, "The Perovskite Fever and Beyond," *Acc. Chem. Res.*, vol. 49, no. 3, pp. 355–356, 2016.

[18] J.-H. Im, C.-R. Lee, J.-W. Lee, S.-W. Park, and N.-G. Park, "6.5% Efficient Perovskite Quantum-Dot-Sensitized Solar Cell," *Nanoscale*, vol. 3, no. 10, p. 4088, 2011.

[19] H.-S. Kim *et al.*, "Lead Iodide Perovskite Sensitized All-Solid-State Submicron Thin Film Mesoscopic Solar Cell with Efficiency Exceeding 9%," *Sci. Rep.*, vol. 2, no. 1, p. 591, 2012.

[20] O. Malinkiewicz *et al.*, "Perovskite Solar Cells Employing Organic Charge-Transport

Layers," *Nat. Photonics*, vol. 8, no. 2, pp. 128–132, Dec. 2013.

[21] J. Burschka *et al.*, "Sequential Deposition as a Route to High-Performance Perovskite-Sensitized Solar Cells," *Nature*, vol. 499, no. 7458, pp. 316–319, Jul. 2013.

[22] J. T.-W. Wang *et al.*, "Low-Temperature Processed Electron Collection Layers of Graphene/TiO 2 Nanocomposites in Thin Film Perovskite Solar Cells," *Nano Lett.*, vol. 14, no. 2, pp. 724–730, Feb. 2014.

[23] D. Liu and T. L. Kelly, "Perovskite Solar Cells With a Planar Heterojunction Structure Prepared Using Room-Temperature Solution Processing Techniques," *Nat. Photonics*, vol. 8, no. 2, pp. 133–138, Dec. 2013.

[24] H. Zhou *et al.*, "Interface Engineering of Highly Efficient Perovskite Solar Cells," *Science* vol. 345, no. 6196, pp. 542–546, Aug. 2014.

[25] W. S. Yang *et al.*, "High-Performance Photovoltaic Perovskite Layers Fabricated Through Intramolecular Exchange," *Science* vol. 348, no. 6240, pp. 1234–1237, Jun. 2015.

[26] M. Saliba *et al.*, "Cesium-Containing Triple Cation Perovskite Solar Cells: Improved Stability, Reproducibility and High Efficiency," *Energy Environ. Sci.*, vol. 9, no. 6, pp. 1989–1997, 2016.

[27] National Renewable Energy Laboratory, "Photovoltaic Research NREL." [Online]. Available: https://www.nrel.gov/pv/.

[28] C. Honsberg and and S. Bowden, "PV Education." [Online]. Available: http://pveducation.org/pvcdrom/solar-cell-structure.

[29] R. Gottesman *et al.*, "Photoinduced Reversible Structural Transformations in Free-Standing CH 3 NH 3 PbI 3 Perovskite Films," *J. Phys. Chem. Lett.*, vol. 6, no. 12, pp.

2332–2338, Jun. 2015.

[30] D. Wang, M. Wright, N. K. Elumalai, and A. Uddin, “Stability of Perovskite Solar Cells,” *Sol. Energy Mater. Sol. Cells*, vol. 147, pp. 255–275, Apr. 2016.

[31] J. Feng and B. Xiao, “Crystal Structures, Optical Properties, and Effective Mass Tensors of CH 3 NH 3 PbX 3 (X = I and Br) Phases Predicted from HSE06,” *J. Phys. Chem. Lett.*, vol. 5, no. 7, pp. 1278–1282, Apr. 2014.

[32] Z. Fan, K. Sun, and J. Wang, “Perovskites for Photovoltaics: a Combined Review of Organic–Inorganic Halide Perovskites and Ferroelectric Oxide Perovskites,” *J. Mater. Chem. A*, vol. 3, no. 37, pp. 18809–18828, 2015.

[33] A. Walsh and G. W. Watson, “The Origin of the Stereochemically Active Pb(II) Lone Pair: DFT calculations on PbO and PbS,” *J. Solid State Chem.*, vol. 178, no. 5, pp. 1422–1428, 2005.

[34] A. Walsh, “Principles of Chemical Bonding and Band Gap Engineering in Hybrid Organic–Inorganic Halide Perovskites,” *J. Phys. Chem. C*, vol. 119, no. 11, pp. 5755–5760, Mar. 2015.

[35] M. R. Filip, G. E. Eperon, H. J. Snaith, and F. Giustino, “With Tunable Optical Band Gaps,” *Nat. Commun.*, vol. 5, pp. 1–9, 2014.

[36] W.-J. Yin, J.-H. Yang, J. Kang, Y. Yan, and S.-H. Wei, “Halide Perovskite Materials for Solar Cells: a Theoretical Review,” *J. Mater. Chem. A*, vol. 3, no. 17, pp. 8926–8942, 2015.

[37] Z. Song, S. C. Watthage, A. B. Phillips, and M. J. Heben, “Pathways Toward High-Performance Perovskite Solar Cells: Review of Recent Advances in Organo-Metal Halide Perovskites for Photovoltaic Applications,” *J. Photonics Energy*, vol. 6, no. 2, p.

22001, Apr. 2016.

[38] S. Bai *et al.*, "High-Performance Planar Heterojunction Perovskite Solar Cells: Preserving Long Charge Carrier Diffusion Lengths and Interfacial Engineering," *Nano Res.*, vol. 7, no. 12, pp. 1749–1758, Dec. 2014.

[39] J. H. Heo, D. H. Song, B. R. Patil, and S. H. Im, "Recent Progress of Innovative Perovskite Hybrid Solar Cells," *Isr. J. Chem.*, vol. 55, no. 9, pp. 966–977, Sep. 2015.

[40] Y. Liu, D. Heinzel, and A. Rockett, "A Revised Version of the AMPS Simulation Code," in *2010 35th IEEE Photovoltaic Specialists Conference*, 2010, pp. 001943–001947.

[41] Y. Liu, D. Heinzel, and A. Rockett, "A New Solar Cell Simulator: WxAMPS," in *2011 37th IEEE Photovoltaic Specialists Conference*, 2011, pp. 002753–002756.

[42] K. Yang, J. R. East, and G. I. Haddad, "Numerical Modeling of Abrupt Heterojunctions Using a Thermionic-Field Emission Boundary Condition," *Solid. State. Electron.*, vol. 36, no. 3, pp. 321–330, Mar. 1993.

[43] G. A. M. Hurkx, D. B. M. Klaassen, and M. P. G. Knuvers, "A New Recombination Model for Device Simulation Including Tunneling," *IEEE Trans. Electron Devices*, vol. 39, no. 2, pp. 331–338, 1992.

[44] "wiki.engr.illinois.edu." [Online]. Available: https://wiki.engr.illinois.edu/display/solarcellsim/.

[45] Simon M. Sze, *Physics of Semiconductor Devices*, 2nd editio. Cham: Springer International Publishing, 2014.

[46] M. Gloeckler, A. L. Fahrenbruch, and J. R. Sites, "Numerical Modeling of CIGS and CdTe Solar Cells: Setting the Baseline," *3rd World Conf. onPhotovoltaic Energy*

Conversion, 2003. Proc., vol. 1, pp. 491–494, 2003.

[47] Y. Wang, Z. Xia, Y. Liu, and H. Zhou, "Simulation of Perovskite Solar Cells with Inorganic Hole Transporting Materials," pp. 3–6, 2015.

[48] B. M. Soucase, I. Guaita Pradas, and K. R. Adhikari, "Numerical Simulations on Perovskite Photovoltaic Devices," in *Perovskite Materials - Synthesis, Characterisation, Properties, and Applications*, InTech, 2016.

[49] A. Zhang, Y. Chen, and J. Yan, "Optimal Design and Simulation of High-Performance Organic-Metal Halide Perovskite Solar Cells," *IEEE J. Quantum Electron.*, vol. 52, no. 6, 2016.

[50] D. K. 5, "Discovery Could Dramatically Boost Eficiency of Perovskite Solar Cells," *Berkeley Lab Res.*, 2016.

VITA

Sai Naga Raghuram Nanduri was born on may20, 1994, in Siddapuram, India. He was educated in in local school St. Francis De Sales High school and graduated from this school in 2009. He completed his B.Tech in Koneru Lakshmaiah University in the year 2015. Later he planned to complete his masters in USA. He attended University of Missouri Kansas city. He completed his masters from University of Missouri Kansas City in 2017. "Numerical simulation and performance optimiztion of perovskite solar cell" paper was published in IEEE PVSC44 conference. Upon completion of his degree requirements, He plans to continue his career in solar design engineer.